Space Sci Rev (2019) 215:33
https://doi.org/10.1007/s11214-019-0598-6

Titan as Revealed by the Cassini Radar

R.M.C. Lopes[1] · S.D. Wall[1] · C. Elachi[2] · S.P.D. Birch[3] · P. Corlies[3] · A. Coustenis[4] · A.G. Hayes[3] · J.D. Hofgartner[1] · M.A. Janssen[1] · R.L. Kirk[5] · A. LeGall[6] · R.D. Lorenz[7] · J.I. Lunine[2,3] · M.J. Malaska[1] · M. Mastroguiseppe[8] · G. Mitri[9] · C.D. Neish[10] · C. Notarnicola[11] · F. Paganelli[12] · P. Paillou[13] · V. Poggiali[3] · J. Radebaugh[14] · S. Rodriguez[15] · A. Schoenfeld[16] · J.M. Soderblom[17] · A. Solomonidou[18] · E.R. Stofan[19] · B.W. Stiles[1] · F. Tosi[20] · E.P. Turtle[7] · R.D. West[1] · C.A. Wood[21] · H.A. Zebker[22] · J.W. Barnes[23] · D. Casarano[24] · P. Encrenaz[4] · T. Farr[1] · C. Grima[25] · D. Hemingway[26] · O. Karatekin[27] · A. Lucas[28] · K.L. Mitchell[1] · G. Ori[9] · R. Orosei[29] · P. Ries[1] · D. Riccio[30] · L.A. Soderblom[5] · Z. Zhang[2]

Received: 13 July 2018 / Accepted: 27 April 2019 / Published online: 21 May 2019

Abstract Titan was a mostly unknown world prior to the Cassini spacecraft's arrival in July 2004. We review the major scientific advances made by Cassini's Titan Radar Mapper (RADAR) during 13 years of Cassini's exploration of Saturn and its moons. RADAR measurements revealed Titan's surface geology, observed lakes and seas of mostly liquid methane in the polar regions, measured the depth of several lakes and seas, detected temporal changes on its surface, and provided key evidence that Titan contains an interior ocean.

✉ R.M.C. Lopes

1 Jet Propulsion Laboratory, California Institute of Technology, 4800 Oak Grove Drive, Pasadena, CA 91109, USA

2 Division of Geological and Planetary Sciences, California Institute of Technology, Pasadena, CA 91125, USA

3 Department of Astronomy, Cornell University, Ithaca, NY 14853, USA

4 LESIA – Observatoire de Paris, CNRS, UPMC Univ. Paris 06, Univ. Paris-Diderot, Meudon, France

5 Astrogeology Science Center, U.S. Geological Survey, 2255 N. Gemini D., Flagstaff, AZ 86001, USA

6 Laboratoire Atmosphères, Milieux, Observations Spatiales (LATMOS), Universite Versaills Saint Quentin, Guyancourt, France

7 JHU Applied Physics Lab, Laurel, MD 20723, USA

8 University of Rome "La Sapienza", Via Eudossiana 18, 00184 Rome, Italy

9 International Research School of Planetary Sciences, Università d'Annunzio, Via Pindaro 42, 65127 Pescara, Italy

10 Department of Earth Sciences, the University of Western Ontario, 1151 Richmond Street, N. London, Ontario N6A 5B, Canada

11 Eurac Research, Institute for Earth Observation, Viale Druso 1, 39100 Bolzano, Italy

12 SETI Institute, 189 Bernardo Ave., Mountain View, CA, USA

13 UMR 5804 LAB, Batiment B18N, University of Bordeaux, allée Geoffroy Saint-Hilaire, 33615 Pessac Cedex, France

As a result of the Cassini mission, Titan has gone from an uncharted world to one that exhibits a variety of Earth-like geologic processes and surface-atmosphere interactions. Titan has also joined the ranks of "ocean worlds" along with Enceladus and Europa, which are prime targets for astrobiological research.

Keywords Titan · Cassini · Radar

1 Introduction

Prior to Cassini, Titan's surface was expected to be strongly influenced by the known presence of methane in a heavy nitrogen atmosphere. Organic compounds and liquid methane, perhaps in the form of vast oceans, were expected in some as yet to be determined relationship with its anticipated ice shell. While the bulk of observational and theoretical work in the decade or so prior to Cassini's arrival emphasized studies of the atmosphere, a number of theoretical investigations were made pertaining to the surface, which were summarized by Lorenz and Lunine (2005). Radar observations using Goldstone and the Very Large Array pointed to an icy (but dirty) surface, but ruled out a deep global ocean of ethane and methane, which were known to be liquids at Titan surface conditions. In addition, HST data and ground-based observations using Adaptive Optics yielded important constraints on the surface, including low resolution maps (Smith et al. 1996) from HST's Wide-Field Planetary Camera 2 that showed a bright region that was subsequently named Xanadu. Titan's surface features and composition were largely unknown, though the surface was thought to be water ice covered with, or mixed with, darker materials such as heavy hydrocarbons and possibly

[14] Department of Geological Sciences, Brigham Young University, Provo, UT 84602, USA

[15] Institut de Physique du Globe de Paris (IPGP), CNRS-UMR 7154, Université Paris-Diderot, USPC, Paris, France

[16] UCLA Department of Earth, Planetary, and Space Sciences, 595 Charles E. Young Dr., Los Angeles, CA 90095, USA

[17] Department of Earth, Atmospheric and Planetary Sciences, Massachusetts Institute of Technology, 77 Massachusetts Avenue, Boston, USA

[18] European Space Agency (ESA), ESAC, Madrid, Spain

[19] Smithsonian National Air and Space Museum, Washington DC, USA

[20] INAF – IAPS National Institute for Astrophysics, Via del Fosso del Cavaliere, 100, 00133 Rome, Italy

[21] Planetary Science Institute, 1700 East Fort Lowell, Suite 106, Tucson, AZ 85719-2395, USA

[22] Department of Electrical Engineering, Stanford University, Stanford, CA 94305-9515, USA

[23] Department of Physics, University of Idaho, Moscow 83843, USA

[24] CNR IRPI, Via Amendola 122/I, 70125 Bari, Italy

[25] Institute of Geophysics, University of Texas at Austin, J.J. Pickle Research Campus, 10100 Burnet Road, Austin, TX 78758, USA

[26] Miller Institute for Basic Research in Science, Department of Earth & Planetary Science, University of California Berkeley, 307 McCone Hall, Berkeley, CA 94720, USA

[27] Royal Observatory of Belgium, 3 Avenue Circulaire, 1180 Brussels, Belgium

[28] Institut de Physique du Globe de Paris, CNRS, 1 rue Jussieu, Paris, France

silicates (Coustenis et al. 1997). Indications of surface liquids were provided by radar observations from Arecibo (Campbell et al. 2003). SAR images from the RADAR instrument were expected to reveal surface geology and location of liquids.

The Titan Radar Mapper (henceforth "RADAR", Elachi et al. 2004) was one of twelve instruments aboard the Cassini spacecraft. It was developed by NASA's Jet Propulsion Laboratory (JPL), the Italian Space Agency (ASI) and the Cassini Radar Science Team primarily to reveal the surface of Titan but also to explore Saturn, its rings and the icy satellites. Nearly opaque at most visible and near-infrared wavelengths, Titan's atmosphere is transparent at RADAR's operating wavelength of 2.17 cm (Ku Band).

While the utility of optical and IR wavelengths was uncertain for a surface investigation due to the atmospheric opacity at short wavelengths, the RADAR instrument was sure to have the capability of penetrating the atmosphere. However, it was selected in the Cassini competition solely as an active experiment with no passive channels. Two passive microwave instruments had been proposed for Cassini with general objectives for observing within the Saturn system, a millimeter/submillimeter spectrometer (MSAR, or Microwave Spectrometer And Radiometer) and a multi-frequency centimeter-wavelength radiometer (SAM, or Saturn Atmospheric Mapper). These experiments were highly rated scientifically but did not make the final selection. Post selection in 1990, the leaders of these proposed investigations, P. Encrenaz, M. Janssen and D. Muhleman, with the help of the RADAR PI C. Elachi, petitioned NASA and ESA to consider adding radiometric capability to the RADAR instrument. The rationale was strictly to support the RADAR investigation of Titan by adding significant capability to the RADAR experiment. A key argument was that this would both support and augment the interpretation of the active data in terms of Titan's surface properties. For example, it was pointed out that the measurement of surface thermal characteristics would allow a new dimension of interpretation. In particular, using the combined passive/active data, the way was opened to obtaining a host of surface thermophysical properties such as composition, density, and structure at depths of a few wavelengths to meters. Among the anticipated results was a surface emissivity map of Titan, from which could be inferred variations in the distribution of oceans and solid surfaces.

The RADAR instrument had therefore four operating modes—synthetic aperture radar (SAR) imaging, altimetry, scatterometry, and radiometry. In its SAR mode, used at altitudes under $\sim$ 4000 km, RADAR imaged Titan's surface at incidence angles from 15 to 35 degrees and spatial resolutions varying as low as 350 m, sufficient to identify major structures and to make geologic maps. SAR mode was occasionally used from higher altitudes ("HiSAR"), yielding coarser spatial resolution ($>$ 1.5 km). SAR images respond to surface roughness scales near the wavelength, to surface slopes at the scale of its resolution, and to dielectric properties of the materials; and they can penetrate many wavelengths into some materials as well, the latter a significant issue on Titan. In addition, radar can penetrate many wavelengths into some materials on Titan, measuring for example the depths of some Titan lakes and seas. SAR images are observationally analogous to optical images and allow us to identify major structures and geomorphologic units.

Altimetry with a range resolution of approximately 30 m results when the antenna is pointed within a fraction of a beam width (0.35 deg) of nadir, at a spatial resolution of the order of 30 km, depending on altitude. The altimetry data have two broad applications.

[29] Istituto di Radioastronomia, Istituto Nazionale di Astrofisica, Via Piero Gobetti, 101, 40129 Bologna, Italy

[30] Dept. Electrical Engineering ad Information Technology, University of Napoli Federico II, Napoli, Italy

First, the aggregate of all data defines an absolute geoid for Titan and constrains any rotational or tidal bulge. Second, relative topographic profiles from each radar pass characterize landforms (e.g., impact craters, mountains), yielding important constraints on geophysical models. Altimetry was obtained over 2% of Titan's surface. In addition, altimetry was able to obtain depths of several lakes and seas (Mastrogiuseppe et al. 2014).

An amplitude monopulse comparison technique called "SARTopo" (Stiles et al. 2009) added an additional 5% topographic coverage (Corlies et al. 2017) of somewhat coarse resolution ($\sim$ 10 km horizontal, $\sim$ 100 m vertical). The SARTopo technique depends on the precise manner in which the location and magnitude of each SAR pixel are affected by variation in surface height between each of the five radar beams (Elachi et al. 2004). Cassini's antenna has multiple beams (feeds), so that specific locations on the ground are observed from two different beams. For different beams, the mislocation error due to surface height is the same, but the magnitude error is different and of opposite sign. The apparent differences in pixel magnitudes between overlapping single beam SAR images are then used to infer height. Nonzero surface heights, therefore, result in apparent differences in pixel positions between overlapping single beam SAR images.

Scatterometry is obtained by pointing the transmitter off-nadir, but processing the echos using the real aperture rather than the synthetic aperture. The data indicate the backscatter efficiency at various incidence angles at relatively low resolution (real aperture resolution depends on range to surface). Scatterometry coverage is near-global (Fig. 1); it can be used as a "basemap" for SAR and as a broad characterization of global terrains. As an independent constraint on surface roughness, scatterometry data are an important complement to radiometry data in order to infer surface composition. In radiometer mode, RADAR collected global measurements of Ku-band brightness temperature with a precision of $\sim$ 0.1 K and an absolute accuracy approaching 1 K (Janssen et al. 2016). Radiometry data consist of antenna temperature measurements that are processed to produce polarized brightness temperatures of the observed scene. The microwave brightness temperature of a solid surface depends on many properties besides physical temperature; e.g., emission angle, polarization, dielectric constant, porosity, surface and subsurface roughness, etc. Making use of surface temperatures independently measured by CIRS (Jennings et al. 2009, 2016), global maps of derived surface properties such as volume scattering and emissivity have been obtained as shown in Figs. 1 and 2. These are described in detail in Janssen et al. (2016).

In its 13-year presence at Saturn, Cassini made a total of 127 passes by Titan, some as close as 880 km. 48 of these were used by RADAR, with one lost in downlink. SAR coverage was limited by both Cassini's orbital path, which used Titan for gravity assists, and by intense competition among instruments for observation time—resulting in a seemingly random set of strips 100–200 km wide (Fig. 3). However, the swaths were chosen to be well distributed in latitude and longitude, allowing for a global picture of the surface to emerge. Areal SAR coverage at the end of mission was 46% using nominal SAR imaging swaths obtained at altitudes below 5000 km with resolutions around 500 m. Coverage increases to 74% when high altitude imaging scans obtained at altitudes above 9000 km are included. High altitude imaging scans have lower resolutions that vary from 1 km to 5 km. Repeat images were obtained over 14% of the surface, and 1.5% was covered four or more times. Real-aperture scatterometry and passive radiometry data exist over the entire surface.

RADAR data, together with near- and mid-infrared images taken by Cassini's Visual and Infrared Mapping Spectrometer (VIMS, Brown et al. 2004) and the Imaging Science Subsystem (ISS, Porco et al. 2004), have given us an opportunity to discover a new world that is both Earth-like and unearthly. We find familiar geomorphology in its mountains, dunes,

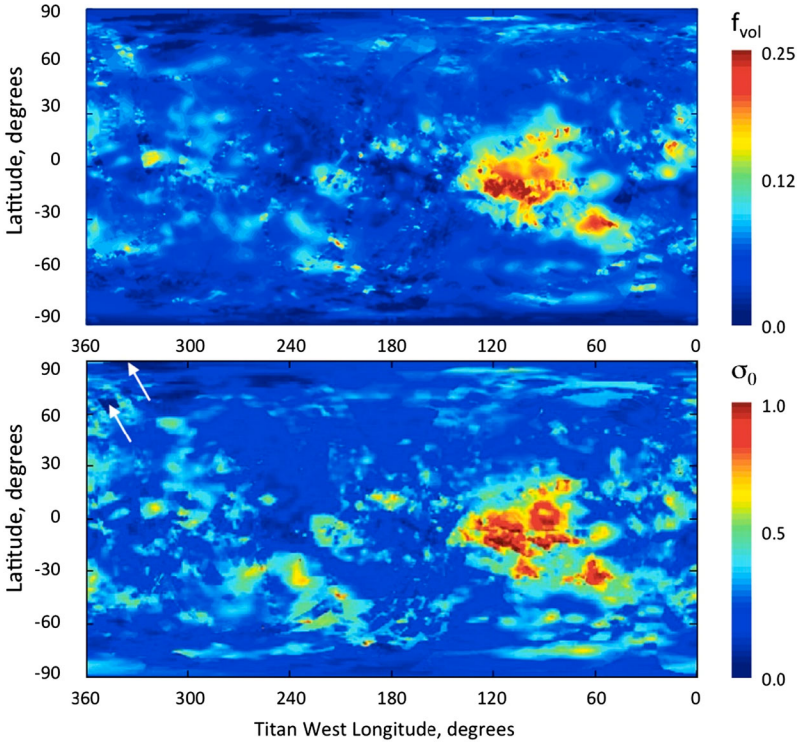

Fig. 1 Predicted and observed maps of scattering from Titan's surface. The upper panel is a map of the volume scattering parameter f_{vol} for a simple surface model composed of a smooth dielectric interface separating free space from an inhomogeneous and isotropically scattering subsurface. f_{vol} is the probability that a photon entering the surface (as determined by the effective dielectric constant) scatters and escapes from the subsurface before it is absorbed. The map of f_{vol} reconciles the maps of effective dielectric constant and emissivity and predicts the overall magnitude of the scattering. The lower panel is a global mosaic of Titan's normalized radar cross-section from all real aperture data through T71 (Wye 2011), showing the actually observed scattering. The white arrows in the upper left-hand corner indicate two small regions that were not mapped

rivers and seas, but note that these features are composed of unfamiliar materials. In this paper, we review RADAR's contributions to geology, hydrology, and surface-atmospheric interaction in an attempt to summarize our knowledge of Titan as obtained from the RADAR instrument at the end of the Cassini mission.

2 Interior

Static and time-varying gravity field measurements (Iess et al. 2010, 2012), rotational dynamics measurements (Stiles et al. 2008, 2010; Lorenz et al. 2008a; Meriggiola et al. 2016) and shape models (Zebker et al. 2009; Mitri et al. 2014; Corlies et al. 2017) have been used to infer the interior structure of Titan. Magnetic field measurements have shown that an intrinsic magnetic field is not present on Titan (Wei et al. 2010). The determination of the rotational dynamics from Cassini RADAR SAR images has been key to constraining the interior structure of Titan. As described above, Cassini RADAR SAR coverage of Ti-

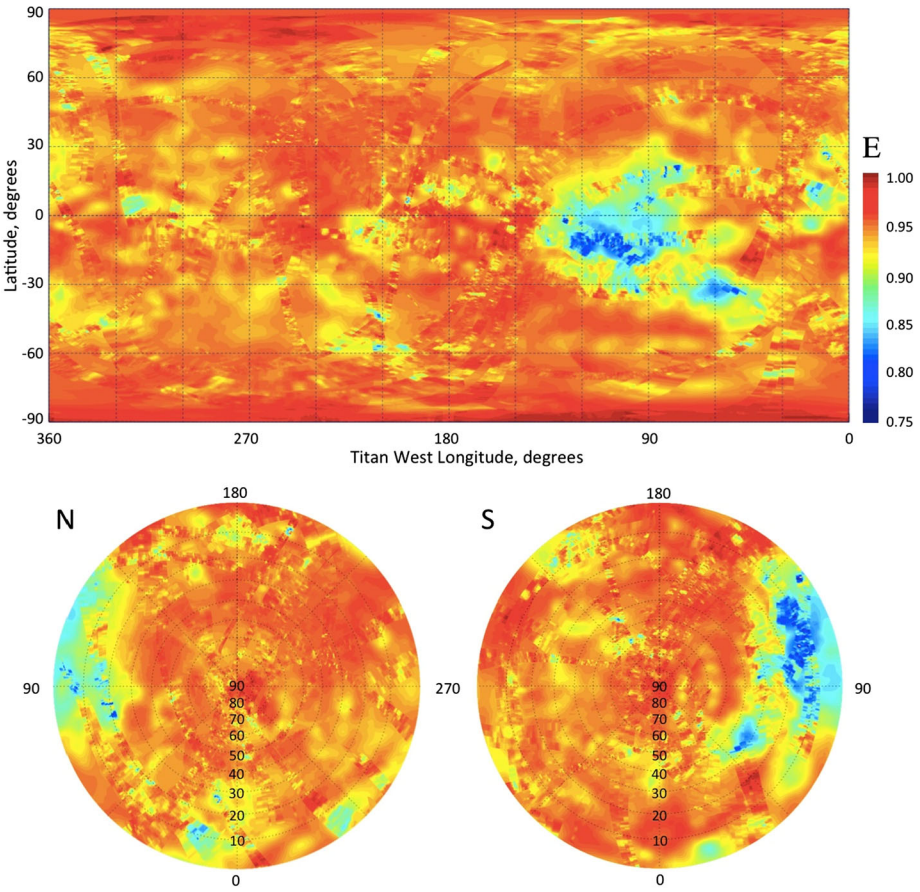

Fig. 2 Global mosaic of emissivity of Titan at the 2-cm wavelength of the Cassini RADAR. This is the final result of the brightness temperature mapping of Titan incorporating all radiometric data obtained from Titan passes, a nearly ten-year span. The brightness temperature was measured as a function of position, polarization and time over a wide range of geometries and ranges, and calibrated to about 1% absolute accuracy using Huygens probe and CIRS temperature measurements as described in Janssen et al. (2016). The polarization data were used to construct a global mosaic of effective dielectric constant, enabling the conversion of all measured brightness temperatures to their equivalent values at normal incidence. The data were then folded into a massive least-squares solution for the seasonally varying brightness temperature distribution of Titan over the time scale of the observations. Comparison with surface temperature measurements obtained in the IR using Kirchhoff's law then enabled the construction of the emissivity map shown. Note that Xanadu, the equatorial region centered on 100 W longitude, is extremely cold and non-emissive, characteristic of a high content of highly fractured water ice bedrock

tan is dependent on orbit dynamics and competition for observation time. As a result, SAR swaths appear somewhat randomly distributed with coincidental overlaps (with only a few exceptions). Where overlap occurs, and assuming that the same surface features appear in both images, it is possible to determine how quickly Titan has rotated between observations and thus estimate Titan's pole location and spin rate (Stiles et al. 2008, 2010), analogous to previous work using Magellan SAR imagery to estimate the spin model of Venus (Davies et al. 1992). First, a set of recognizable landmarks observed in two different SAR images obtained at different times is located in a Titan-centered inertial, non-rotating (J2000) refer-

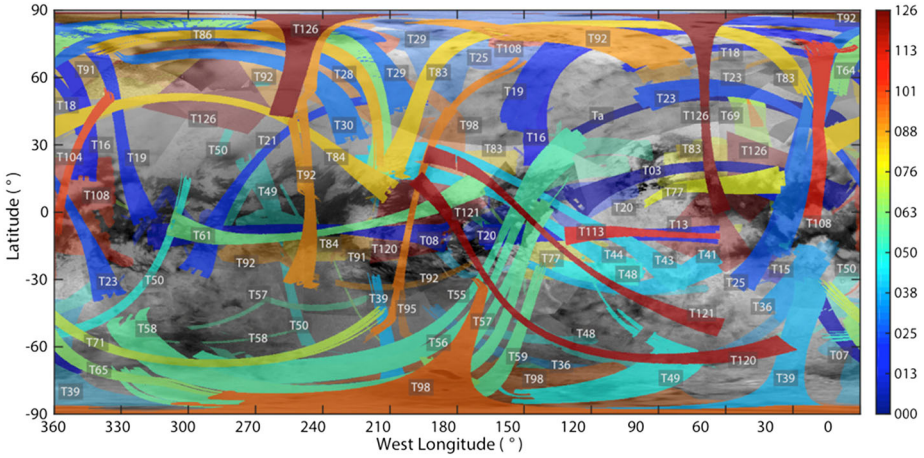

Fig. 3 Combined Titan SAR coverage from the entire Cassini mission. Swaths are shown over an ISS basemap. The swaths colors, displayed on the right-hand side, represent Titan flyby numbers

ence frame. Pixels chosen in each SAR image, corresponding as closely as possible to the same point on the landmark, are aligned using several techniques to minimize landmark mismatches. The spin state parameters are estimated by minimizing the misregistration error—that is, the apparent movement in Titan body-fixed coordinates of the landmarks between observation times. Feature mapping is much more robust for radar than for passive optimal imagery, because radar geolocation is independent of spacecraft pointing knowledge except that the general direction (within 10 degrees or so) must be known to exclude ambiguous returns from the opposite side of the spacecraft. Accurate radar pixel locations in inertial space depend only on the accuracy of the measurement of delay, Doppler shift, spacecraft velocity and position, and presumed target body topography. Nearby SARTopo (Stiles et al. 2009) measurements of topography help determine more precisely variations in feature locations in inertial space. Using similar methodology and a more extensive set of observations, Meriggiola et al. (2016) also provided a rotational model of Titan estimating the spin pole location, the spin rate, the precession and the nutation. Further, these authors show that the pole location is compatible with the Cassini state 1 (a dynamical equilibrium wherein the spin axis, the orbit normal and the normal to the invariable plane are coplanar).

Stiles et al. (2008) and Meriggiola et al. (2016) have provided an estimate of Titan's obliquity (0.31°). The obliquity together with the quadrupole moment of the gravity field (J_2 and C_{22}) measurements (Iess et al. 2010, 2012) constrain the moment of inertia of Titan. These results were used by Bills and Nimmo (2011) to estimate the radial mass distribution of Titan and, when combined with the low-degree gravity field derived from Cassini spacecraft Doppler tracking data (Iess et al. 2010), suggest that Titan's outer shell is mechanically decoupled from the deeper interior. Bills and Nimmo (2011) and Meriggiola et al. (2016) find that the estimated obliquity is compatible with a deep interior decoupled from the outer ice shell by a global subsurface ocean. The presence of a subsurface ocean inferred from the rotational dynamics of Titan is consistent with the large tidal response of Titan (tidal Love number $k_2 = 0.589 \pm 0.150$) (Iess et al. 2012; see also Mitri et al. 2014). In agreement with this scenario, the Permittivity, Wave and Altimetry (PWA) subsystem of the HASI (Huygens Atmospheric Structure Instrument) on board the Huygens probe measured a Schumann-like resonance, also suggesting the presence of a subsurface ocean (Béghin

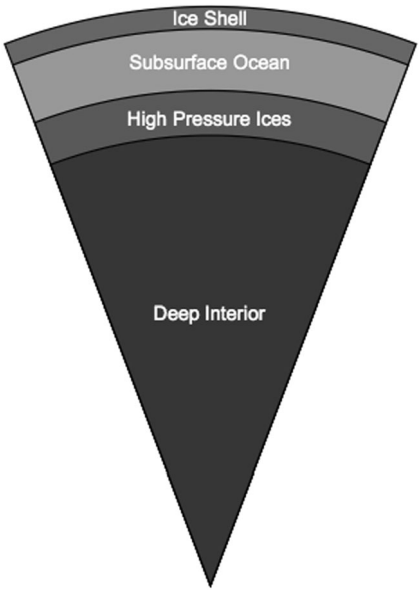

Fig. 4 Probable present-day structure of Titan's interior showing that Titan is internally differentiated, with a deep rocky or rock-ice mix deep interior

et al. 2012). In summary, the gravity, topography and rotational dynamics measurements in combination with thermal-evolution models indicate that Titan is internally differentiated (Fig. 4), and has an outer ice shell, a subsurface ocean, a high pressure layer at the base of the ocean, and a deep rocky or rock-ice mix interior (Hemingway et al. 2013; Mitri et al. 2014; Tobie et al. 2014).

3 Global Shape

Cassini RADAR observations using both the altimetry and SARTopo modes reveal Titan's global shape and yield insights to its interior structure. The roughly 60 satellite-derived elevation surface traces (Fig. 5; Zebker et al. 2009) show that Titan's polar radius is less than, and the equatorial radii are greater than, predicted by its gravity field. Best-fitting solutions are shown in Table 1 below.

The hydrostatic ratio $(a - c)/(b - c)$, which is exactly 4 for a spin-locked satellite in hydrostatic equilibrium (Hemingway et al. 2018), for Titan's figure is observed to be only 2.14 (Zebker et al. 2009; Corlies et al. 2017). The hydrostatic ratio obtained from the third degree gravity observations is 3.83, that is, the gravity field reflects approximate hydrostatic equilibrium. While the gravity field is consistent with a hydrostatically relaxed body, Titan's figure is not. If both of these data constraints pertain, Titan's interior does not conform to a set of spherically symmetric shells, as these data imply that the average satellite density at the equator is less than at the poles. If Titan has a vast interior ocean of liquid water, then some ice layers (less dense than liquid water) are thinner at the poles than the equator. A simple model satisfying both sets of data and assuming isostatic compensation (Fig. 6) could be the result of uneven heat dissipation in Titan's interior, such as may result from tidal interaction with Saturn or its other moons.

Another possible explanation for the overly oblate topographic figure is that there is greater precipitation of hydrocarbon snow or loosely packed hydrocarbon particulates at the

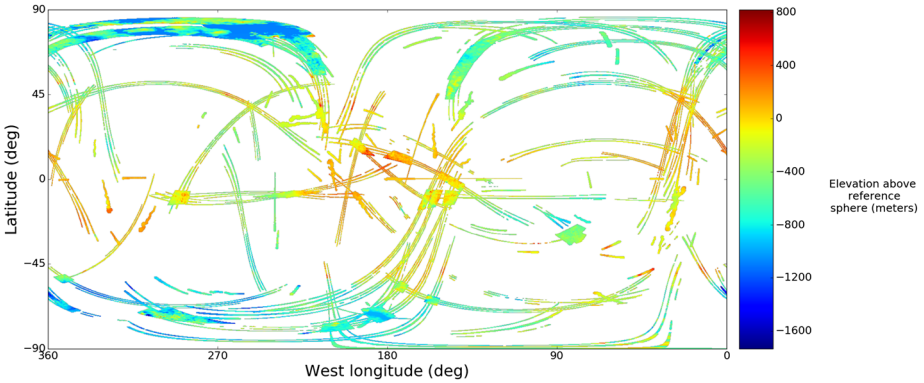

Fig. 5 Cassini measurements of Titan surface height above a reference sphere of 2575 km radius. As expected, the shape is dominantly triaxial ellipsoidal, with topographic lows near the poles and topographic highs at the prime- and anti-meridians. However, the polar flattening is greater than expected for a hydrostatic body, meaning the equatorial topography stands higher than expected and the polar depressions are lower than expected, suggesting that the depth to the subsurface ocean is smaller at the poles than at the equator

Table 1 Titan gravity and shape triaxial ellipsoids (m)

	Gravity	Elevations	Difference
a axis	2574875 ± 7.3	2575124 ± 26	−249
b axis	2574716 ± 7.4	2574746 ± 45	−30
c axis	2574660 ± 4.5	2574414 ± 28	246
a translation	0.8 ± 5.6	69.8 ± 6.2	
b translation	0.1 ± 5.6	68.3 ± 8.0	
c translation	1.7 ± 3.9	45.8 ± 6.4	
Mean eq. rad.	2574795	2574761	−34
Hydrostatic ratio $(a-c)/(b-c)$	3.83	2.14	

equator than at the poles, perhaps with a net equatorward transport from the poles, which would also be consistent with the data (Zebker and Wong 2016). This could account for increased distance from the surface to the planet center at the equator if sufficient material were so transported. We note that this is consistent with the observation of 100-m tall dune structures near Titan's equator (see Sect. 5.3), so that poorly consolidated material may indeed collect there to a greater extent. Several hundred meters of deposition at the equator would match the mean equatorial radii of both models, but precipitation would have to preferentially occur in the sub- and anti-Saturnian directions, which seems unlikely.

Further comparisons of the gravity and shape observations can constrain the depth of any outer ice shell enclosing a global subsurface ocean (Zebker and Wong 2016). While the exact value varies depending on how the spherical expansion is constrained, the observed gravity to topography ratio is 0.070 for the third order terms and 0.042 for fourth order (Zebker and Wong 2016). These preliminary results suggest ice-shell thicknesses of 327 and 187 km, respectively, a factor of ≥ 2 more than the 100 km expected from thermal models (Sohl et al. 2003; Nimmo and Bills 2010) and interpretation of the Schumann resonance

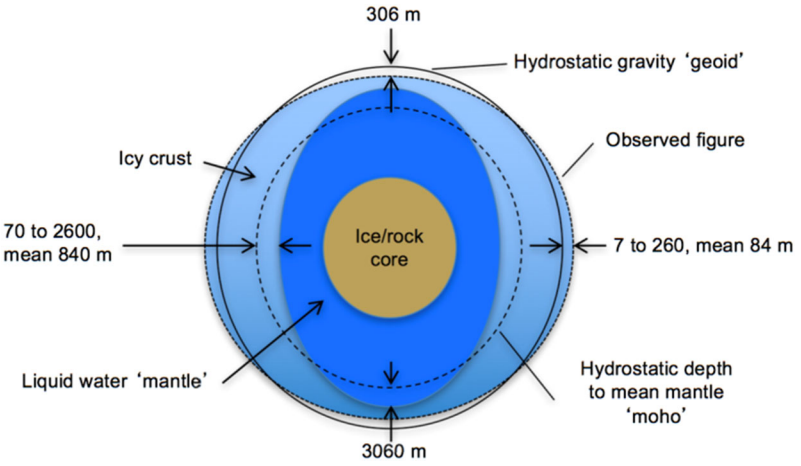

Fig. 6 A model consistent with Cassini gravity and figure measurements, assuming isostatic compensation. The thinner ice shell (exaggerated for visibility in the figure) at the poles could result from uneven heat dissipation within Titan from tidal interactions, and the relatively shallower "geoid" at the poles is one explanation for the preponderance of lakes at the most northern and southern latitudes. The shallower geoid allows mobile liquids to lie closer to the surface

observations by the Huygens probe (Béghin et al. 2012). The Zebker and Wong solution yields a tidal Love number h_{2t} of about 0.5, and a basal heat flow of 2.5 mW/m^2. This would suggest that heat from Titan's deep interior is lower than often assumed, hence the amount of radiogenic material in the deep interior is likely less as well. These data also constrain the depth of Titan's subsurface ocean and density of its deep interior, placing added restrictions on its composition and evolution. Supposing that Titan has an undifferentiated ice/rock deep interior beneath the ocean, and that the moment of inertia is most likely in the range 0.33–0.34 (Iess et al. 2010), then the $\sim$ 200-km-thick ice shell estimate above and Titan's well-known mean density of 1.88 g cm^{-3} implies an ocean depth (thickness of the subsurface ocean layer) and deep interior density ranging from 308 km and 2.74 g cm^{-3} (MOI = 0.33), to 226 km and 2.55 g cm^{-3} (MOI = 0.34).

4 Composition and Surface and Subsurface Properties

The Cassini-Huygens mission has revealed the surface of Titan in unprecedented detail, enabling us to discern different geomorphological units on the surface (Sect. 5), constrain the relative times of emplacement of these units, and place constraints on composition. Titan has an ice shell (Fig. 4) but water ice signatures are not easily detected due to atmospheric scattering and absorption that hamper the observations and the presence of complex organic molecules on the surface. The extended, dense, and hazy N_2-CH_4 dominated atmosphere shields the surface from direct optical observations, except at certain wavelengths where the methane absorption is weak. These methane "atmospheric windows" (McCord et al. 2006) are exploited by the Cassini VIMS to obtain compositional information of the top few microns of the surface, as discussed in Sect. 4.2 below, while RADAR can probe the surface and subsurface scattering properties, and hence place additional constraints on composition.

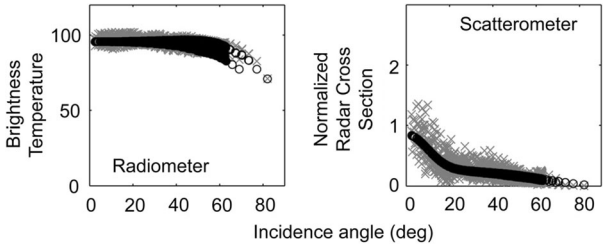

Fig. 7 Angular dependence of radiometer (left) and scatterometer (right) measurements of a portion of Titan's surface. Grey x's are observations, while black circles are modeled values assuming both surface and volume scattering terms. Both sets of curves fall off slowly with incidence angle, indicative of significant volume scattering

4.1 Surface and Subsurface Scattering Properties

Compared to the surfaces of the Moon or the Earth, the off-nadir radar response from most of Titan's surface is quite strong at Ku-band ($\lambda = 2$ cm). This indicates that more complex processes than simple surface scattering, such as a significant volume scattering component, have to be considered (Elachi et al. 2005; Wye et al. 2007; Paganelli et al. 2007; Janssen et al. 2016). Indeed, given the low Titan surface temperatures and the low loss tangent of analogs of materials relevant to Titan's surface, signals from Cassini RADAR's Ku-band instrument should penetrate the surface down to a depth ranging from a few decimeters for an organic and compacted near-surface, to several meters for a pure water ice near-surface (Paillou et al. 2008) and thus have multiple opportunities to be scattered. The above referenced observations of Titan's surface are consistent with sub-surface volume scattering processes, in addition to pure surface scattering. Analysis of Cassini scatterometer and radiometer measurements obtained simultaneously (see Fig. 7) are best fit using models where volume scattering, enabled by the low material losses, is enhanced by coherent backscatter processes (Zebker et al. 2008; Janssen et al. 2011).

Janssen et al. (2016) further advance that a regionally enhanced degree of volume scattering is indicative of a higher abundance of water ice in the near-surface. This is because water ice is more transparent to microwaves than common organic materials, allowing for more opportunities for scattering. This would be consistent with about 10% of Titan's near-surface being water ice-rich while the composition of the remaining terrains is dominated by more absorbing organic materials, likely by-products of the intense atmospheric photochemistry (Lorenz et al. 2008b; Hörst 2017). The regions that contain a high degree of volume scattering include mountainous terrains, impact craters, fluvial and fan-like features, all of which possibly correspond to highly fractured or unconsolidated sedimentary materials derived from erosion. Some of these materials could also have originated from cryovolcanism, in which the radar signature could be explained by a strong volume scattering effect in a thick water-ammonia ice layer using a two-layer scattering model (Paillou et al. 2006). Radar-bright sinuous channels in the southwest of Xanadu (Sect. 5.8), showing very large radar cross-sections, are also consistent with the presence of icy, low-loss, rounded scatterers, acting as efficient natural retro-reflectors (Le Gall et al. 2010).

Weaker radar reflectors such as Titan's dunes are most likely organic in nature (as also supported by VIMS (e.g., Barnes et al. 2008; Soderblom et al. 2009; Clark et al. 2010)). However, we note that these features exhibit somewhat high backscatter at large incidence angles compared to Earth analogs, which suggests even aeolian sediments may contain centimeter-scale gravels producing a significant volume scattering component (Paillou et al. 2014). Features interpreted as mega-yardangs were observed on Titan, and they also exhibit

a much brighter radar signature than their terrestrial analogs, indicating that additional scattering processes, such as volume scattering, occur in those materials as well (Paillou et al. 2016).

Lastly, and of particular interest, is the case of Titan's methane-dominated lakes, where radar waves can penetrate down to several thousand wavelengths (at least 150 m) and be subsequently backscattered by the bottoms of a lake or seabed (Mastrogiuseppe et al. 2014). These results are consistent with recent laboratory investigations of the electrical properties of liquid hydrocarbons (Mitchell et al. 2015).

4.2 Surface Composition from VIMS and RADAR

A combination of RADAR and near-infrared multispectral imaging data (VIMS) is a powerful way to distinguish and categorize geomorphological features into units with distinct chemical compositions (that remain to be identified). Spectroscopic observations of Titan's surface are severely hindered by the presence of an optically thick, scattering and absorbing atmosphere, allowing direct investigation of the surface within only a few spectral windows in the near-infrared longward of 1 μm. Based on the 1.29/1.08 μm, 2.03/1.27 μm, and 1.59/1.27 μm band ratios measured by VIMS at low to moderate latitudes, several main spectral units were initially distinguished on the surface of Titan. These include material, informally referred to as, the "equatorial bright" material, mainly distributed in the topographically high and mid-latitude areas, the "dark blue" material adjacent to the bright-to-dark boundaries, the "dark brown" material, which correlates with RADAR-dark dune fields, and the "Xanadu" material, which comprises the bright regions of Xanadu (Barnes et al. 2007a; Soderblom et al. 2007; Jaumann et al. 2008).

Even though these spectral units are distinct, their actual compositions remain elusive. A number of chemical species were proposed to exist on the surface of Titan, but only a few absorptions were unambiguously detected from remote-sensing observations carried out by VIMS during Cassini flybys. A methane-ethane dominated composition seems to be present in the polar lakes and seas of Titan (e.g., Brown et al. 2008; Lunine and Lorenz 2009). IR spectroscopy, microwave radiometry and scatterometry are sensitive to the physical structure of the surface to a different extent and at different scales. IR spectroscopy measurements are used to determine surface composition, but they are also affected, down to depths of micrometers, by the physical properties of the surface material like roughness, photometric geometry, and porosity.

Correlations between near-infrared and microwave data of Titan's surface are useful to gather a broader understanding of surface properties. These were quantified at coarse spatial resolution by Tosi et al. (2010), who applied a multivariate statistical analysis to an aggregated data set made up of infrared spectra acquired by VIMS at spatial resolution of tens of km together with scatterometry and radiometry data measured by RADAR. This technique allowed for the identification of regional surface units at equatorial to mid-latitudes. Some of these units matched both the major dark and bright features seen in the ISS mosaic of Titan (Porco et al. 2005; Turtle et al. 2009), whereas other units showed boundaries not apparent from the visible and near-infrared remote-sensing data set. In particular, while dark equatorial basins are very similar to each other in terms of infrared and microwave reflectance at this spatial scale, the major bright features do not share the same characteristics.

A comprehensive investigation of Titan's surface features using the VIMS and RADAR-SAR datasets at the best available spatial resolution is still the best approach to characterize geomorphologic units using both spectral and morphologic characteristics. For example, the correlation between the 5-μm-bright materials and RADAR empty lakes suggests the presence of sedimentary or organic-rich evaporitic deposits in dry polar lakebeds (Barnes et al.

2011a; MacKenzie et al. 2014). Langhans et al. (2012) extensively studied the morphology, distribution, and spectral properties of Titan's fluvial valleys showing that these are mostly associated with the bright surface unit.

In recent years, several investigators have applied radiative transfer models in addition to comparison between data sets (e.g., Hirtzig et al. 2013; Solomonidou et al. 2014; Lopes et al. 2016; Bonnefoy et al. 2016). These studies allow definition of both the surface and the atmospheric contributions from VIMS spectral imaging data after performing the appropriate pixel selection of areas of interest with the help of SAR data.

The application of radiative transfer analyses to the VIMS Titan data yields extracted weighted surface albedos in the seven methane windows (weighted averages of the VIMS channels per window; Solomonidou et al. 2016), which have been tested against a variety of Titan candidate ice and organic constituents to provide constraints on the possible material present in various geomorphological units (Solomonidou et al. 2018). An updated material library is being used based on Bernard et al. (2006), Brassé et al. (2015) and the GhoSST database (http://ghosst.osug.fr). This library includes several materials at different grain sizes, such as ices of acetylene (C_2H_2), ethylene (C_2H_4), ethane (C_2H_6), propane (C_3H_8), cyanoacetylene (HC_3N), water (H_2O), ammonia (NH_3), methane (CH_4) and carbon dioxide (CO_2), in addition to spectra of laboratory tholins (Bernard et al. 2006; Brassé et al. 2015), and spectra of dark materials such as asphalite, kerite, different types of anthraxolite and amorphous carbon, which have been proposed to lower the total surface albedo of Titan's surface (Lellouch 2006; GhoSST database). Considering the different grain sizes, the library consists of 148 different constituent possibilities that can also be mixed. By using this constituent library, spectral simulations are made, and an iterative process is used to obtain the best fit to the observations, bearing in mind that there is no unique solution for the whole mixtures. With these and other caveats, Solomonidou et al. (2018) have derived constraints on the possible major constituent for each geological unit and reported a latitudinal dependence of Titan's surface composition, with water ice being the major constituent at latitudes poleward of 30°N and 30°S, while Titan's equatorial region appears to be dominated by a very dark organic material, possibly aromatic in character (Clark et al. 2010). The surface albedo differences and similarities among the various geomorphological units also have implications for the geological processes that govern Titan's surface and interior (e.g. aeolian, cryovolcanic, tectonic).

5 Surface Geology

5.1 Major Geologic Units and Mapping

SAR data have been used since the early days of the mission to interpret different types of terrains (Fig. 8; Stofan et al. 2006; Paganelli et al. 2007, 2008; Lopes et al. 2010). More recent work used not only SAR data but added correlations with data from other RADAR modes (altimetry, SARTopo, scatterometry and radiometry), and also from VIMS and ISS to provide sufficient information on Titan's surface to distinguish the major types of terrain units (Malaska et al. 2016a; Lopes et al. 2016). These data were also used to establish the major geomorphologic unit classes on Titan and their relative ages using contacts between units. In order of total surface area, the classes of units are: plains, dunes, hummocky terrains, labyrinth terrains, lakes, and impact craters. The oldest units are the hummocky and the labyrinth terrains; it is not possible with currently available data to differentiate the relative ages of these two oldest types of terrain. The hummocky terrains consist of mountain

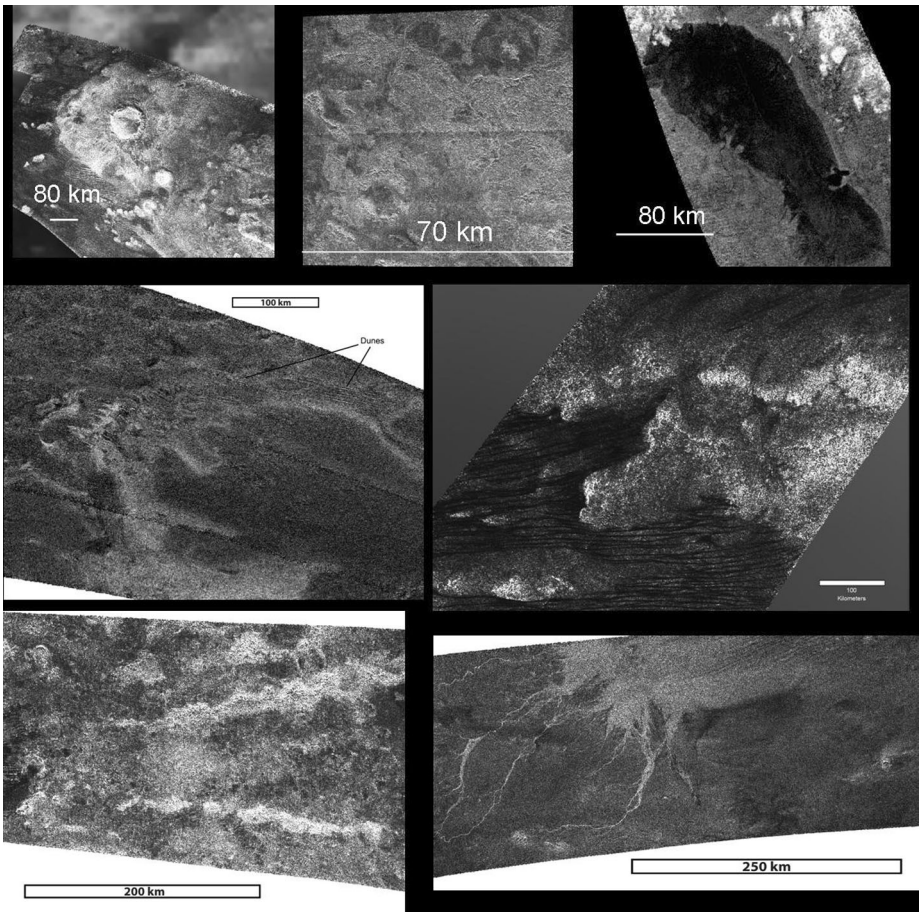

Fig. 8 Examples of geologic features on Titan: Top row from left: Sinlap crater with its well defined ejecta blanket. Middle: Crateriform structure (suspected impact crater) on Xanadu. Right: Ontario Lacus near Titan's south pole. Middle row, left: Bright (high radar backscatter) deposit Winia Fluctus abutting darker undifferentiated plains, the dunes indicated by arrows overlie part of deposit. Middle row, right: Dunes abutting against hummocky and mountainous terrain. Bottom left: mountains (radar bright) in the equatorial region. Right: Elivagar Flumina, interpreted as a large fluvial deposit, showing braided radar-bright channels which overlie radar-dark undifferentiated plains

chains and isolated radar-bright terrains. The labyrinth terrains consist of highly incised and dissected plateaus with medium radar backscatter. The plains are younger than both mountainous/hummocky and labyrinthic unit classes. Dunes and lakes of liquid hydrocarbons are the youngest unit classes on Titan. Additionally, we have identified individual features such as crater rims, channels, and candidate cryovolcanic features. Crater rims and candidate cryovolcanic features are locations more likely to expose materials from the icy shell, while the hummocky/mountainous materials are thought to be exposed remnants of the icy shell's surface.

Characterization and comparison of the properties of the unit classes and individual features with data from radar radiometry, ISS, and VIMS provide information on their composition and possible provenance and shed light on the interconnection between the interior,

the surface, and the atmosphere. Both microwave emissivity and VIMS are helpful in characterizing the units, although they have different penetration depths, with microwave emissivity penetrating tens of cm into the surface, while infrared-based responses, such as VIMS and ISS, penetrate only the top surface coating on the order of microns. From microwave emissivity data described above, the hummocky/mountainous terrains and impact crater rim features have relatively low emissivity (and greater radar scattering) in radiometric data, consistent with more water ice near the surface (Fig. 2). The undifferentiated plains, dunes, labyrinth terrains, and lakes all have high emissivity (lower radar scattering) in radiometric data which is consistent with low-dielectric organic materials.

Spectral coatings of the terrain units, following early studies by McCord et al. (2008), Barnes et al. (2007b), were described in Solomonidou et al. (2018) and discussed above. From this analysis, three groups of compositional mixtures are reported, which include the major geomorphological units mentioned in the previous section, among three candidates (water ice, tholin, and a dark component). The units with spectral responses most similar to water ice are the labyrinth terrains and a number of different types of plains such as the streak-like, the scalloped, and the undifferentiated plains that are concentrated at the higher parts of the mid-latitudes. The impact crater ejecta examined (6 in Solomonidou et al. 2018) and the alluvial fans (5 in Solomonidou et al. 2018) are part of a different compositional group in which a tholin-like material is dominant. Furthermore, the units covered with an unknown dark constituent are the hummocky/mountainous terrains, the variable plains, the dunes, and the undifferentiated plains that are close to the equator and possibly contaminated by dune material (Lopes et al. 2016; Solomonidou et al. 2018). Since microwave radiometry and VIMS are global datasets, although at lower spatial resolution than SAR, we can also use these correlations to extrapolate to regions not covered by SAR. This is particularly important as SAR data did not provide complete coverage of Titan at the end of the Cassini mission.

5.2 Plains

Plains are the most widespread type of terrain on Titan (Lopes et al. 2016). Although there are several different types of plains, by far the most extensive are the Undifferentiated Plains, first mapped by Lopes et al. (2010). These are vast expanses of radar-dark terrains that appear fairly uniform in SAR images, with no major topographic units and are for this reason often referred to as “blandlands”. Lopes et al. (2016) mapped the distribution of the Undifferentiated Plains using SAR swaths up to flyby T92 (July 2013) and found that these terrains are located mainly at mid-latitudes. Their gradational boundaries and paucity of recognizable features in SAR data make geologic interpretation challenging, so Lopes et al. (2016) used all the RADAR datasets available, plus VIMS and ISS, to examine and evaluate different formation mechanisms including (i) cryovolcanic origin, consisting of overlapping flows of low relief or (ii) sedimentary origins, resulting from fluvial/lacustrine or aeolian deposition, or accumulation of photolysis products created in the atmosphere. Their analysis showed that exposures of Undifferentiated Plains in the lower mid-latitudes are consistent with a composition predominantly containing organic rather than icy materials and formed by depositional and/or sedimentary processes, unlike the undifferentiated plains in the higher mid-latitudes, which are consistent with water ice (Solomonidou et al. 2018). The study concluded that aeolian processes played a major part in the formation of the Undifferentiated Plains, though other processes (fluvial, deposition of photolysis products) are likely to have contributed, possibly in differing proportions depending on location. However, the distribution of Undifferentiated Plains, both at local and global scales, is consistent with aeolian deposition being the major process contributing to their formation.

Fig. 9 Dunes on Titan as seen by the Cassini SAR (wavelength 2.17 cm, with spatial resolution of 350 m) in the Belet Sand Sea, from the T61 (Aug. 2009) swath on the equatorial leading hemisphere, at 11°S, 255°W. Dune surfaces are generally smooth and absorbing to SAR and thus typically, as here, appear as SAR-dark lines against a rougher and/or fractured, and thus radar-bright substrate, unless the RADAR is pointed directly at a dune face, in which case it appears as a thin, SAR-bright line. Occasionally the radar incidence is such as to give bright glints (specular reflection) from dune slopes. The open arrows indicate the direction of SAR illumination and incidence angle. From Radebaugh (2013)

Spectral differences between the Plains and Dunes seen in VIMS data imply that the materials, at least on the top layers of the surface, are not exactly the same. Spectral differences in terms of surface albedo values between locations of Undifferentiated Plains (Lopes et al. 2016; Solomonidou et al. 2018) show that Plains at lower latitudes (closer to the dune seas) are more spectrally similar to dune materials, suggesting that they are related and supporting the idea that dune materials are transported by wind from equatorial to mid-latitudes (Malaska et al. 2016a). The Undifferentiated Plains located at lower mid-latitudes (and therefore closer to the equatorial dunes) appear to be composed predominantly of organic materials, which may have been cemented by an organic substance and/or wetted by methane, causing them to become spectrally different from dune materials, at least at a surficial level. Work by Malaska et al. (2016a) and Lopes et al. (2016) suggests that the plains deposits may be derived from modified dune materials—thus tying two of the major geomorphologic units together. If the Undifferentiated Plains materials are mainly the result of aeolian deposition but contain liquids due to methane rain or fluids transported by channels, this could explain why they show relatively high emissivity (lower global dielectric constant, less efficient volume scattering) as well as why they are free of observable dunes (reduced sediment mobility). It would also be consistent with the high level of degradation of craters found at mid-latitudes, potentially due to efficient erosion by fluvial, pluvial, or subsurface flow activity (Neish et al. 2016).

5.3 Dunes

One of the youngest and most areally extensive geomorphologic units on Titan consists of sand dunes (Lorenz et al. 2006). These appear as long, narrow, and SAR-dark features against a SAR-brighter substrate or interdune (Fig. 9), presumably because dune sands are smooth to RADAR at the 2.17 cm Cassini SAR wavelength. The dunes are generally 1–2 km wide, spaced by 1–4 km and can be over 100 km long (Lorenz et al. 2006;

Radebaugh et al. 2008). Limited measurements of heights from radarclinometry suggests they are 80–130 m tall (Neish et al. 2010). They are grouped together in large dune fields, or sand seas, equatorward of ±30 degrees latitude. Titan's dunes interact with topographic obstacles, seen as SAR-bright and generally isolated mountains, in a way that indicates general W-E transport of sand; they pile up on the west side of obstacles, divert in their azimuth around the obstacles, and are sparser on the east side (Radebaugh et al. 2010). Their size, general morphology and relationship with underlying terrain and obstacles, and their style of collection are nearly identical to large, linear dunes in Earth's sand seas of the Sahara, Arabia and Namibia (Lorenz et al. 2006; Radebaugh et al. 2008; Le Gall et al. 2011, 2012). Such dunes on Earth typically form under bimodal winds (Fryberger and Dean 1979; Tsoar 1983). A more recent model calls on a dominant, slightly off-axis wind and a secondary wind causing sand flux down the dune long axis (Courrech du Pont et al. 2014; Lucas et al. 2014).

Regardless of whether the classical (bimodal) or fingering-mode dune growth mechanisms apply, a fundamental challenge raised by the RADAR observations of the dunes is the eastward direction of growth and sand transport (Lorenz et al. 2006; Radebaugh et al. 2010). This contrasts with expectations that low-latitude near-surface winds should generally blow to the west. The solution appears to be that the dunes reflect strong but infrequent eastward winds, either associated with vertical mixing in the atmosphere at equinox leading to strong westerly gusts (Tokano 2010) or methane rainstorms having a similar effect (Charnay et al. 2015). Additionally, convergence of the meridional transport predicted in models (e.g. Lucas et al. 2014) can further explain why Titan's dunes are confined within ±30° latitudes, where sediment fluxes converge (see also Malaska et al. 2016a).

Titan's dune sands are not only dark to SAR but they are some of the darkest materials seen by ISS (Porco et al. 2005; Karkoschka et al. 2017) and have a low albedo and red slope as seen by VIMS, thus comprising the VIMS "dark brown" spectral unit (Soderblom et al. 2007; Barnes et al. 2008; Clark et al. 2010; Rodriguez et al. 2014). Volume scattering within the dunes is very low, consistent with smooth, homogeneous surfaces in general, and lacking large voids or clasts (Janssen et al. 2009; Le Gall et al. 2011), although modeling by Paillou et al. (2014) suggests shallow surface ripples and some volume scattering. The observations indicate that the dunes cannot be composed primarily of water ice, but rather must be dominated by organics, presumably derived from photolytic processing of methane in the upper atmosphere, and precipitation to the surface (Lorenz et al. 2006, 2008a; Soderblom et al. 2007). Sand sources could include river channels, as on Earth (Radebaugh 2013); or the midlatitude blandlands, though it's also possible that sands are being transported there from the equatorial regions (Lopes et al. 2016; Malaska et al. 2016a). The extent of the dunes indicates that sands have been generated on Titan in great volumes and transported by wind, and that processes have acted on the surface long enough to produce extensive and morphologically consistent landforms (Radebaugh 2013). Bonnefoy et al. (2016) extracted distinct dune and interdune spectra and emissivities from most of Titan's major dune fields. Their results indicate sand-free interdune areas of varying composition, implying that the sand dunes have been active on geologic recent timescales.

Gathering all exploitable SAR and HiSAR images since the start of the Cassini mission, Rodriguez et al. (2014) built a global map of the dune coverage available at that time, accounting for observations from TA to T92 flybys (from October 2004 to July 2013) and more than 30 individual RADAR SAR and HiSAR swaths. They evaluated that dunes cover $13 \pm 2\%$ of the 58.1% of Titan's surface observed with SAR and Hi-SAR, considering only those images having sufficient spatial resolution to identify individual dunes (i.e., excluding

HiSAR swaths with a resolution coarser than 2 km/pixel). In terms of latitudinal distribution, 99.6% of the imaged dunes are found within the equatorial belt (within ±30° latitudes), 61.3% of which has been imaged after flyby T92. The overlapping of a VIMS global mosaic and the global distribution of dunes as seen by the RADAR highlights the strong correlation between the dunes and a specific infrared unit spectrally compatible with complex solid organics (the "dark brown" unit). This allowed an extrapolation of the dune geographic distribution to the entire spatial extent of the VIMS dark brown unit, even in locations where dunes are not seen because of lack of RADAR coverage, and extending the previously estimated total surface area of Titan covered by dunes up to ≈ 17% (≈ 14.10^6 km^2, 1.5 times the surface area of the Sahara desert on Earth), the same as early estimates from Lopes et al. (2010). A simple calculation of the volume (e.g. Lorenz et al. 2008b; Rodriguez et al. 2014) indicates that dunes are a major surface reservoir of organics, probably originating from the atmosphere.

In addition to dunes, there are other aeolian features and landforms on Titan's surface. These are wind streaks and yardangs, or wind-carved ridges. The wind streaks are visible in ISS images as bright features that extend in the downwind direction from obstacles (e.g. Porco et al. 2005; Lorenz et al. 2006; Malaska et al. 2016a). They can be several tens of kilometers wide and long, can have flow-like, teardrop shapes, and appear as though wind has shaped the bright landscapes, and has deposited dark materials, likely sand, in the low regions downwind of the obstacles. These features help indicate the direction of the winds, which also broadly parallels the linear dunes seen in Cassini SAR images (Malaska et al. 2016a).

Deposits that are SAR-bright, circular in planform and likely elevated into small mounds or domes are found in some regions in the northern midlatitudes (Lopes et al. 2016). These domes are easily eroded as revealed by deep, badlands-like river channels that flow outwards from their centers. Cutting across the channels and the domes are a series of parallel, long lineations ∼ 1 km wide, spaced by a few km, and tens of kilometers long (Paillou et al. 2016; Northrup et al. 2018). They are similar in appearance and SAR brightness, radiometry and scatterometry to yardangs, or wind-carved ridges (Paillou et al. 2014). These appear to have formed in easily eroded materials, similar to yardangs on Earth and Mars and further indicate the action of wind at moderate to high latitudes now or in the past (Northrup et al. 2018).

5.4 Impact Craters

Before Cassini arrived at Saturn, the impact cratering history on Titan was unknown from direct observations, though it was generally assumed that Titan had a similar impact crater production history as the other Saturnian satellites. Estimates of the cratering rate were made by extrapolating the crater distributions observed on other Saturnian satellites, or by predicting impact rates by comet populations. Such estimates suggested that at least several hundred craters larger than 20 km in diameter should be present on Titan (Zahnle et al. 2003). Impactors that create craters smaller than 20 km in diameter are expected to be disrupted by Titan's atmosphere and not result in craters (Artemieva and Lunine 2005; Korycansky and Zahnle 2005). Cassini RADAR observations show an extreme paucity of craters. Only 23 certain or nearly certain craters and ∼ 10 probable craters > 20 km in diameter have been observed on Titan, with a handful of smaller crater candidates (Wood et al. 2010; Neish and Lorenz 2012; Buratti et al. 2012; Neish et al. 2016). This suggests that Titan has a crater retention age of several hundred million years to a billion years (Wood et al. 2010; Neish and Lorenz 2012), with the oldest surfaces located near the equator and the youngest surfaces located near the poles (Neish et al. 2016).

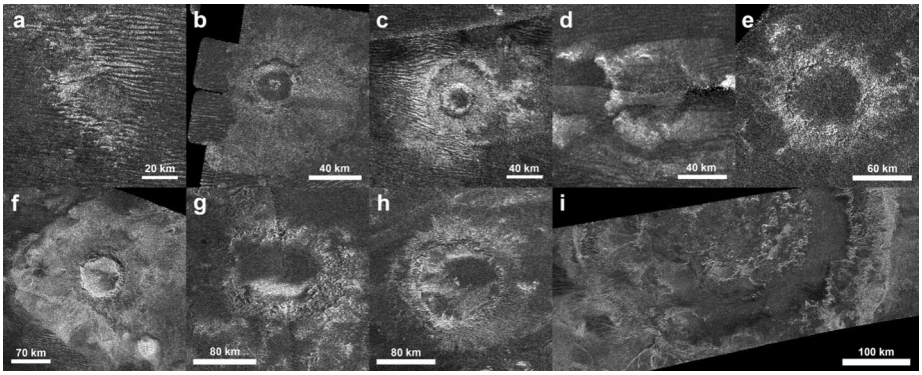

Fig. 10 Nine probable impact craters observed on Titan by Cassini RADAR, from smallest (**a**) to largest (**i**). Impact craters on Titan show modification by exogenic processes such as fluvial erosion and infilling by sand. Figure from Neish et al. (2013)

The craters that are observed on Titan all show evidence for extensive modification by erosional processes (Fig. 10). Channels are observed to cut through the ejecta blankets and floors of several impact craters (Wood et al. 2010; Soderblom et al. 2010; Neish et al. 2015). Many of Titan's impact craters are located in its equatorial sand seas, and also show evidence for extensive infilling by sand (Wood et al. 2010; Le Mouelic et al. 2008; Neish et al. 2013). In addition to the morphologic evidence for erosion and burial, Titan's craters are consistently shallower than similarly sized fresh craters on Ganymede (often by many hundreds of meters), suggestive of infill (Neish et al. 2013). Given the distribution of depths, aeolian infilling appears to be the dominant modification process on Titan (Neish et al. 2013), but fluvial erosion seems to play an important secondary role (Neish et al. 2016). Modification by viscous relaxation is expected to be minimal given the cold lithospheric temperatures on Titan ($\sim$ 90 K), although insulation by sand could enable some relaxation in Titan's larger craters (Schurmeier and Dombard 2018).

In addition to being highly modified, Titan's impact craters are not uniformly distributed across the moon. There is an almost complete absence of impact craters near Titan's poles, with the majority of the craters found in the topographically high, equatorial sand seas (Neish and Lorenz 2014). There have been several hypotheses advanced to explain this observation. Neish and Lorenz (2014) proposed the lack of craters near Titan's poles might be indicative of marine impacts into a former ocean in this region. Moore et al. (2014) suggested that extreme climate change occurred in Titan's recent past, causing global methane rainfall that produced sediment that settled in Titan's topographically low polar regions, burying any craters there. Finally, Neish et al. (2016) suggested that an increased rate of fluvial erosion near the poles could degrade Titan's craters to the point where they would be unrecognizable from orbit. In any case, Titan's cratering record demonstrates that it is an extremely dynamic world, and studying its impact structures can reveal much about the processes that have shaped it.

5.5 Mountains and Tectonics

Features of relatively high topography, termed mountains, have been observed across Titan (Fig. 11). Large topographic relief on icy satellites is rare, taking the form of, for example, impact crater rims, grooved terrain on Ganymede, or the towering scarps of Miranda. This

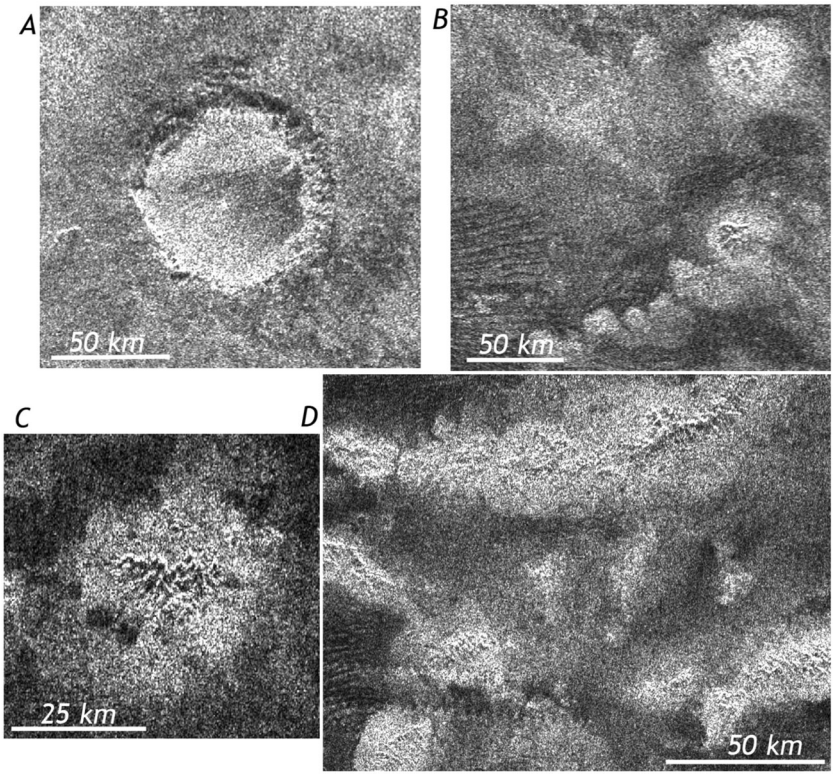

Fig. 11 Some examples of mountains on Titan. Radar illumination is from the top in all cases, and north is up. Bright, possibly erosional, blankets surround the central, high elevation features visible as bright/dark pairs. (**a**) Sinlap Crater, shown to demonstrate the effects of radar illumination on a rimmed depression. (**b**) Individual mountain blocks in the T3 swath south of Sinlap crater. (**c**) Rugged mountain from the T3 swath. (**d**) A portion of mountain ranges west of the Huygens landing site from the T8 swath. From Radebaugh et al. (2007)

is in part because water ice generally loses strength with increasing depth, making high topographies difficult to support rigidly. However, the exceptional amount of erosion on Titan may also be responsible for terrain height reduction. Overall, topography on Titan is rather subdued, having a range of just a few kilometers (Lorenz et al. 2013; Corlies et al. 2017); nevertheless, there are features on the surface aside from impact crater rims that are elevated. These take the form of isolated blocks, chains, ridges, and elevated plateaus (Radebaugh et al. 2007). Mountains of all types are SAR-bright due to the roughness and fractured nature of the materials, as well as the slope geometry with respect to the SAR antenna look direction and incidence angle. Mountains also exhibit high scattering and have a high emissivity as seen by RADAR (Janssen et al. 2009, 2016), and are part of the VIMS bright blue unit (Barnes et al. 2007b), indicating a higher water-ice component, the dominant material of Titan's lithosphere.

Isolated mountain blocks are found only in a few select regions and tend to be several km across and a few hundred meters high, as observed by radarclinometry (Radebaugh et al. 2007). More frequently, mountains are found in small belts near the middle and high latitudes, and are only few to tens of kilometers in length, and also a few hundred meters high. In terms of area, mountain chains are the most extensive rugged fea-

tures (aside from Xanadu) and are the most dramatic on the surface, being found dominantly at the equatorial regions and generally aligned E-W. They are up to several hundred kilometers in length, are arcuate in planform, and can be up to several kilometers high (Radebaugh et al. 2007, 2016). In Xanadu, there are extensive, mountainous and rugged terrains. These appear crenulated to SAR and exhibit multiple overlapping peaks concentrated in regions over tens to hundreds of square kilometers. They are interspersed with lineations that indicate a regional tectonic fabric, likely extensional, given the straight nature of the lineations (Radebaugh et al. 2011). All mountains on Titan are highly rugged and exhibit signs of extensive erosion from methane rainfall and possibly mass wasting. All mountain ridges and chains exhibit a preferential orientation (Cook-Hallett et al. 2015; Liu et al. 2016a) indicating internal tectonic forces operating on their formation. The equatorial mountain chains differ in morphology from long, narrow tectonic features on other icy satellites: they sit on elevated topography (Radebaugh et al. 2016), they are arcuate in morphology, and they have low slopes (Liu et al. 2016b). This indicates they are more likely to have been created by contractional tectonism, by N-S directed forces in the interior and at the equator. Such thrust faulting could have been enabled by liquid methane within the ice shell, which could act to lubricate fault zones, much as occurs on Earth with water (Liu et al. 2016b). A similar conclusion is reached for the mountain ridges north of Xanadu, which contain the highest peak on Titan at just over 3300 m (Radebaugh et al. 2016), that they were formed by contractional tectonism (Mitri et al. 2010). Some very large-scale tectonic rises, several hundred kilometers across, may be as uplifted and later dissected plateaus composed of organic sedimentary materials (Undifferentiated Plains) that are the surface expression of large subsurface laccoliths (Schurmeier et al. 2017).

5.6 Cryovolcanism

Cryovolcanism involves the eruption of materials that would ordinarily be solid at the surface temperature of the icy bodies of the outer Solar System: cryomagmas therefore include liquid or gaseous water or aqueous solutions, possibly mixed with solid fragments (Lopes et al. 2013a). The existence of features on Titan formed by cryovolcanic activity has been the subject of some controversy, which is unlikely to be resolved by Cassini data, mainly due to imagery and spatial coverage limitations (Nixon et al. 2018). The possibility of finding cryovolcanic features on Titan had been discussed prior to Cassini (e.g. Lorenz 1993, 1996). The case for cryovolcanism was strengthened by results from the Gas Chromatograph Mass Spectrometer (GCMS) instrument on board the Huygens probe, which detected the radiogenic isotope of Argon (^{40}Ar) in Titan's atmosphere (Niemann et al. 2005) in concentrations suggesting that the atmosphere was in communication with a reservoir of the parent atom, ^{40}K. Prior to the first Titan flyby using RADAR, VIMS imaged a bright feature (later named Tortola Facula) that Sotin et al. (2005) proposed to be cryovolcanic in origin. Sotin et al. (2005) further suggested that the upwelling of large cryovolcanic plumes might be releasing sufficient methane into the atmosphere to account for the known atmospheric composition. However, SAR images obtained later in the mission showed Tortola Facula to be a local topographic high similar to others elsewhere on Titan (Lopes et al. 2013b) and not a candidate for a cryovolcanic feature.

Cassini RADAR and VIMS revealed several features interpreted as formed by cryovolcanism (Barnes et al. 2006; Sotin et al. 2005; Lopes et al. 2007; Nelson et al. 2009a, 2009b; Soderblom et al. 2009; Wall et al. 2009; Lopes et al. 2013b; Solomonidou et al. 2016). However, the interpretation has been debated (e.g., Moore and Pappalardo 2011) and has not been entirely resolved by Cassini data (Nixon et al. 2018), primarily due to limitations

in spatial resolution and coverage. Cryovolcanic interpretations by RADAR (using several data sets including SAR, stereogrammetry (Kirk et al. 2010), SARTopo, and radiometry) and VIMS (surface albedo retrievals, surface composition constraints, and temporal variations) are based on morphology; differences in surface albedo between the cryovolcanic areas, their surrounding terrains, and several other geomorphological features; and possible temporal variations detected by VIMS (Barnes et al. 2005; Nelson et al. 2009a, 2009b; Solomonidou et al. 2014, 2016, 2018). However, the Cassini mission had limited repeated coverage of the cryovolcanic candidate features and those observations did not reveal any hot spots (thermal enhancements) that would have provided conclusive proof of active cryovolcanism. The detection of thermal activity at Titan's surface using radiometry data (which is sensitive to variations of ~ 1 K) or VIMS, would require Cassini's instruments to be observing the right locations at the right times and in multiple occasions, an unlikely scenario given the consensus that cryovolcanic candidate features are not ubiquitous on Titan (Lopes et al. 2010, 2013b; Nixon et al. 2018).

Landforms considered as possibly cryovolcanic include flow-like terrains seen on the western margin of Xanadu (Wall et al. 2009), spectrally different regions in Tui Regio (Barnes et al. 2005) and tangled flow regions in Hotei Regio (Soderblom et al. 2009; Wall et al. 2009). These flow-like morphologies even exhibit elevated, lobate margins typical of flows. Other possible cryovolcanic features are the steep-sided, small lakes at the north polar region (see Sect. 5.9). These landforms have slightly elevated rims, steep sides, flat floors, and deposits diffuse to SAR surrounding them. All of these characteristics are typical of maar craters on Earth (Wood et al. 2007) though they are also generally consistent with dissolution and sublimation-related features (Hayes et al. 2017).

The strongest evidence for cryovolcanic features on Titan was put forward by Lopes et al. (2013b) who combined SAR imaging (including stereogrammetry, Fig. 12) and VIMS data (Fig. 13) for a region that includes two mountains, Doom Mons (40.4°W, 14.7°S) and Erebor Mons (36.2°W, 5.0°S), as well as a depression, Sotra Patera (40.0°W, 14.5°S), and a region consisting of flow-like features, Mohini Fluctus (centered at 38.5°W, 11.8°S). Doom and Erebor Montes are tall mountains (Doom being ~ 70 km in diameter and 1.5 ± 0.2 km high, Fig. 12), Sotra Patera is the deepest depression found on Titan (1.7 ± 0.2 km deep, relative to surrounding terrain). It is non-circular and interpreted as a collapse feature adjacent to Doom Mons (Fig. 13). Mohini Fluctus appears to emerge from Doom Mons. Other non-circular, collapsed depressions are located between the two Montes, and flow-like features also surround Erebor Mons.

A criticism by Moore and Pappalardo (2011) of initial interpretations by RADAR of cryovolcanic candidates reported by Lopes et al. (2007) is that flow-like features could have been produced by fluvial activity, since channels are seen in areas such as Hotei Regio and Ganesa Macula (where topography later obtained by RADAR showed was not a shield or dome as initially interpreted). However, the Doom Mons–Sotra Patera–Erebor Mons region is totally devoid of visible fluvial channels, making a fluvial origin for Mohini Fluctus and other flows unlikely. A vast dune field is located between Doom and Erebor Montes, indicating a dry region. The depressions seen in the region, including Sotra Patera, are not circular, are very deep, and are therefore unlikely to have had an impact origin (Lopes et al. 2013b). VIMS data analysis has contributed to the cryovolcanic interpretation via two different types of investigation. First, analysis of VIMS data using a radiative transfer model (Solomonidou et al. 2014) showed that the surface albedo of the candidate cryovolcanic features is different from that of plains or dunes, indicating differences in composition (Solomonidou et al. 2014). Following this and again using a radiative transfer model on a large selection of VIMS data, Solomonidou et al. (2016) revealed temporal changes for the Sotra Patera and Mohini

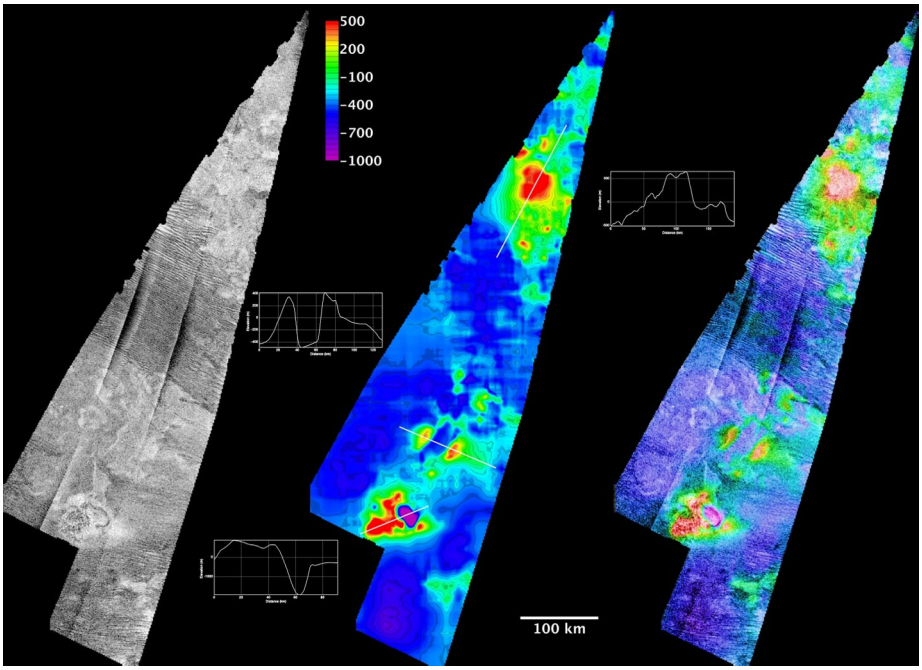

Fig. 12 Topography of Doom Mons, Sotra Patera and (at the top) Erebor Mons region from SAR stereo. The image on the left is SAR over the region. The central image shows a color-coded DTM (scale shown), with the tops of Doom and Erebor Montes being the highest points. The white lines show the locations of the three profiles shown. The SAR and DTM are merged at the right. (From Lopes et al. 2013b)

Fluctus area, which became brighter up to a factor of 2 in terms of pure surface albedo and brightness during one year (2005–2006), while surrounding areas and the undifferentiated plains and dunes did not present any significant change for the same period of time. The surface albedo variations, together with the presence of volcanic-like morphological features consistent with volcanism, suggest that the regions might be active and possibly connected to the deep interior via cryovolcanic processes. Additional support for cryovolcanic origin of these features comes from interior structure models of Titan and corresponding calculations of the spatial pattern of maximum tidal stresses (Sohl et al. 2014), which indicate that the Doom Mons–Sotra Patera–Erebor Mons area is a likely region for cryovolcanic activity. Other putative cryovolcanic regions on Titan were discussed by Lopes et al. (2013b).

5.7 Labyrinth

The enigmatic labyrinthic terrains of Titan are defined as elevated highly dissected plateaus with intersecting valleys or remnant ridges of low to medium backscatter with a generally > 5000 km^2 extent (Malaska et al. 2010; Moore et al. 2014; Malaska et al. 2016b, 2017a). The Katain Labyrinth (Fig. 14) is a typical example. SARTopo data suggest that labyrinth terrains are among the locally highest units on Titan (Stiles et al. 2009). Often the valley floors contain radar-dark floors or fill. The valley and upland widths are variable: in areas where the valleys are narrow and the intervening uplands (or valley spacing) are wide, the terrain appears in the form of a dissected plateau; when the widths of the valleys and the widths of the intervening plateaus are about equal, the terrain appears as a series of valleys

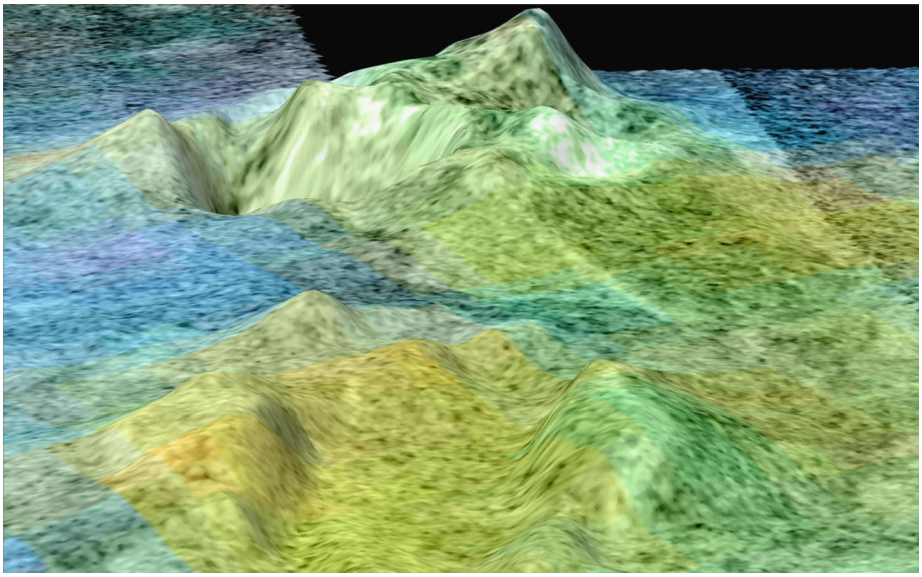

Fig. 13 Perspective view of Doom Mons and Sotra Patera, obtained by combining a Digital Topographic Model (produced from two SAR swaths) and VIMS data showing compositional differences in representative color, which shows that the dune fields (in blue) are of a different composition from the candidate cryovolcanic materials in shades of green and yellow. The image shows one of the tallest peaks on Titan, Doom Mons, which is ~ 70 km in diameter and 1.5 ± 0.2 km high. Doom Mons is adjacent to the deepest depression so far found on Titan, Sotra Patera, an elongated pit ~ 30 km in diameter and 1.7 ± 0.2 km deep. The DTM data have a vertical exaggeration of 10:1. A movie showing the whole region can be seen at: http://photojournal.jpl.nasa.gov/catalog/PIA13695

and intervening plateaus; and when the valleys are wide and the widths of the intervening plateaus are small, the terrain can appear as a series of remnant ridges. Closed valleys (having no external drainage) may also be present, although this may be a result of the coarse resolution of the Cassini RADAR.

Wide valleys are suggestive of amphitheater-headed valleys. The overall planforms of the labyrinth terrain units are circular, ovoid, or tabular. The valley density at a scale of 300 m/pixel is above 0.02, significantly higher than the density of valley networks described elsewhere on Titan such as the network in western Xanadu (Burr et al. 2009). The valley networks inside the labyrinth units are rectangular to dendritic, suggesting varying amounts of structural and topographic control. Some of the more circular planform labyrinths have valley or ridge networks that are radial, extending away from the center of the region, suggesting that doming occurred prior to erosion, possibly as a result of a liquid water laccolith injection at depth (Schurmeier et al. 2017, 2018). At the terminus of the valley networks and in contact with the labyrinths, undifferentiated plains units are found, suggesting a close connection between the two types of units, at least at the local scale.

Radiometry data suggest that the labyrinth terrains consist of a possibly uplifted thick plateau of organic materials. The emissivity data show that labyrinth terrains have significantly higher emissivity than mountain and hummocky terrains and have similar emissivities to dunes or undifferentiated plains. The microwave data are consistent with the labyrinths being composed of low dielectric organic materials and are not consistent with materials containing significant amounts of water ice. However, VIMS analysis of one labyrinth region

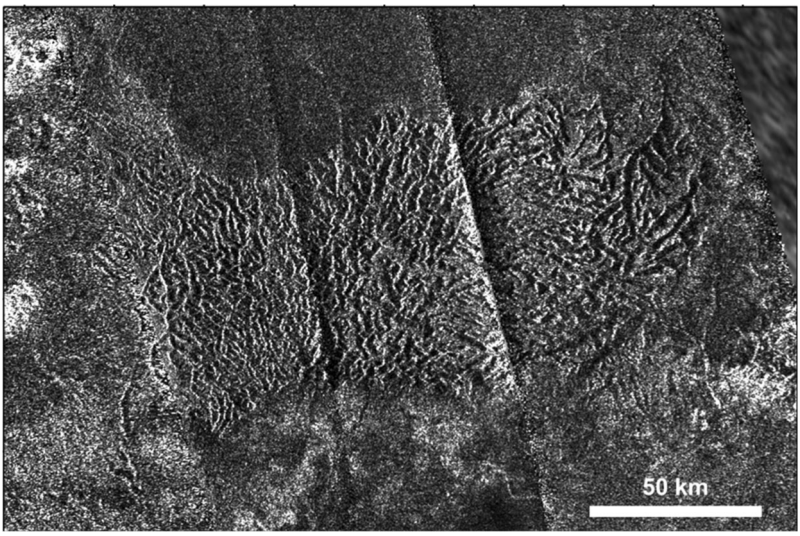

Fig. 14 SAR image of Katain Labyrinth. (52N, 349W) The highly dissected feature at center is Katain labyrinth. SAR illumination is from right (large straight lines through center are SAR artifact due to beam overlap). Sinusoidal projection centered at 349W. North is at top

(Solomonidou et al. 2018) show that, at least on the top surface, the material is compatible with water ice as the major constituent.

The labyrinths were likely formed from the uplifted plateaus through a combination of dissolution coupled with mechanical erosion, or other phase changes that could allow the development of closed valleys with transport of the remaining materials to the outlying plains. Karstic dissolution is a likely scenario, and many of the labyrinth terrains have morphologic analogs with terrestrial karst terrains (Malaska et al. 2010). Theoretical predictions and laboratory work have shown that organic materials on Titan may dissolve when exposed to Titan hydrocarbon rainfall or liquids. (Raulin 1987; Lorenz and Lunine 1996; Cordier et al. 2009; Malaska et al. 2011a; Glein and Shock 2013; Malaska and Hodyss 2014; Cornet et al. 2015, 2017). Dissolution geology on Titan may create a landscape that is similar to terrestrial karst terrain present in water-soluble materials such as limestone and gypsum on Earth (Malaska et al. 2011a; Malaska and Hodyss 2014; Cornet et al. 2015). Preliminary modelling by Cornet et al. (2017) suggests that blocks of Titan soluble materials could dissolve under Titan conditions to form the features observed by SAR that are similar to polygonal karst. The evolution sequence begins with incised valleys in a plateau, then widening to form the end-stage wide-floored remnant ridges. Type examples of each stage are found in close proximity near Sikun Labyrinth in Titan's south polar terrain and are shown in Fig. 15. However, other formation scenarios are possible, including differential hardening and deflation, aeolian deflation, or other phase change and removal processes such as sublimation. From superposition relations, the labyrinths represent an ancient terrain (Malaska et al. 2016b), emplaced prior to the undifferentiated plains (Lopes et al. 2016).

5.8 Xanadu

Much of Titan's geology has a regional organization; dunes and mountain belts are found near the equator, lakes and seas are found near the poles, and relatively bland regions are

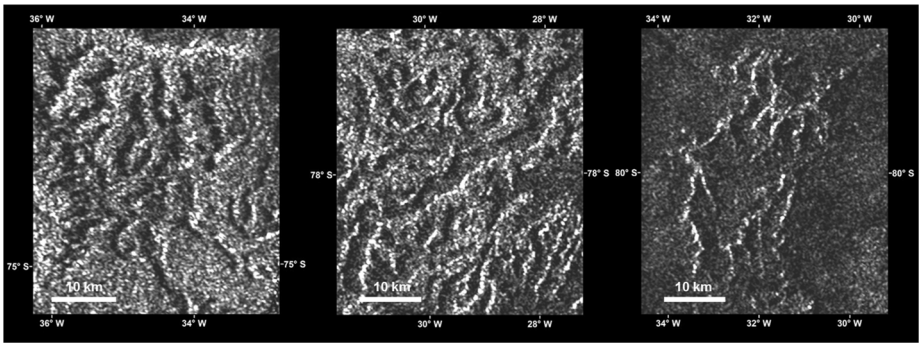

Fig. 15 SAR images of different types of labyrinth terrains found in close proximity in Titan's south polar terrain. Left: Naraj Labyrinth, represents thin valleys incised in a plateau, Center: Sikun Labyrinth, represents valleys and plateaus of near equal width, Right: Tupile Labyrinth, a type example of remnant ridge. Sinusoidal projection. North is at top

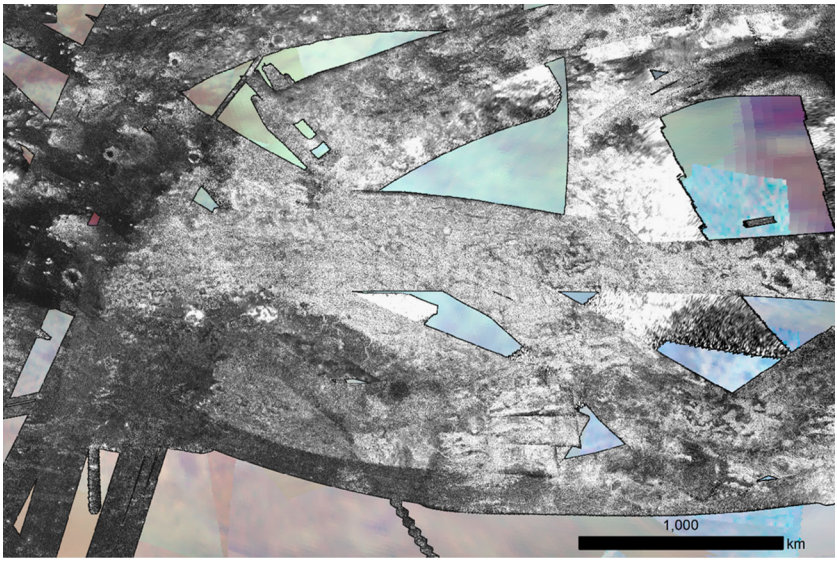

Fig. 16 Xanadu region. All Cassini SAR and HiSAR image swaths covering the Xanadu region, overlain on a VIMS basemap. Xanadu is generally SAR-bright because of rough terrain and fractured ice, which is interspersed with valleys filled with SAR-darker sediment. Some regions of Xanadu are VIMS dark blue, consistent with the presence of exposed water ice. The southwest margin of Xanadu has large river channels emptying to the south

located in the midlatitudes (Lopes et al. 2010). Xanadu (Fig. 16), however, is a continent-sized region that breaks with all predictions. It is 4000 × 2500 km wide, is located on Titan's leading hemisphere, and interrupts the equator-encircling sand seas. The feature was observed before Cassini arrived (Lemmon et al. 1993; Smith et al. 1996), and efforts were made to observe and understand Xanadu by Cassini SAR and other instruments. Xanadu is generally SAR-bright, which indicates it is composed of rough and fractured terrains (Radebaugh et al. 2011). It has a high backscatter but low emissivity as indicated in scatterometry and radiometry measurements, which is consistent with a water-ice composition

in the bedrock (Wye et al. 2007; Zebker et al. 2008; Janssen et al. 2009, 2016). Furthermore, some portions of Xanadu are correlated with the VIMS dark blue unit, indicating there is a higher than average percentage of water-ice exposed at the surface (Barnes et al. 2007a; Tosi et al. 2010).

Xanadu is unique in several respects to other regions on Titan. While geologically diverse, many regions in Xanadu have extremely rugged terrains, manifest as many adjacent, deeply eroded, and incised mountain ranges (Radebaugh et al. 2011). There are broad-scale linear features characteristic of NE-SW and NW-SE extensional tectonism, and broadly arcuate mountain ranges indicative of N-S directed contractional tectonism (Radebaugh et al. 2011). These features all indicate a long and complicated tectonic history for Xanadu. Extensive, dendritic networks of varying morphologies (Burr et al. 2009), large channels that distribute fans and cobbles to the south (Le Gall et al. 2010), and the extensive erosion of the mountains also reveal a long erosional history. Over twice as many impact craters or possible impact craters can be found in Xanadu as on the rest of Titan (Wood et al. 2010; Radebaugh et al. 2011), which is further evidence of the generally old nature of Xanadu compared with the rest of the surface of Titan (Radebaugh et al. 2011; Wood et al. 2010). A region of mottled terrain is found on the western margin, with arcuate depositional morphologies and lack of integrated drainage, postulated to be a possible cryovolcanic deposit (Wall et al. 2009). These morphologies are consistent with other possible cryovolcanic zones in Hotei Regio, bordering Xanadu's southern margin (Soderblom et al. 2009). These landforms may instead be related to swamp-like deposits entirely fluvial in origin, but they are unique and not widespread.

Xanadu's most puzzling characteristic is that despite the abundance of mountains and high local topographic variations, the region as a whole appears to be regionally lower in elevation than anywhere else near the equator (Zebker et al. 2009; Stiles et al. 2009). This is evidenced by radar altimetry measurements as well as SARTopo observations (Stiles et al. 2009). It is possible that after a time period of mountain-building and contraction, there was gravitational collapse of the water ice shell (Mitri et al. 2010), resulting in broad extensional tectonism and down-dropping of Xanadu (Radebaugh et al. 2011). This scenario might have led to Xanadu-bounding fault zones, along which the possible cryolavas of western Xanadu and Hotei in the south could have ascended (Radebaugh et al. 2011). What could have driven this N-S directed contractional tectonism is unknown but might have resulted from global contraction related to interior cooling, tidal spinup or spindown, or internal convection (Radebaugh et al. 2011).

Several outstanding questions about Xanadu remain, in addition to its origin: why is it regionally depressed? Why the dunes of the equatorial sand seas do not cover and fill Xanadu? Why is water ice more exposed here than in most other places on Titan? Much remains to be learned about this unusual region.

5.9 Lakes

While ISS revealed $\sim$ 50 dark features poleward of 70°S during one of Cassini's first observations of Titan, these features were not initially referred to as lakes as they could not be distinguished from dark equatorial dune fields at optical wavelengths (Porco et al. 2004). The first high-resolution and definitive observations of Titan's hydrocarbon lakes were acquired by the RADAR in July 2006 (T16), when $\sim$ 75 features with exceptionally low backscatter, high emissivity, and distinctly lacustrine morphology were identified in SAR images (Stofan et al. 2007). The confirmation that the lakes contained liquids was obtained by VIMS observations showing specular reflection from one of the lakes (Stephan et al. 2010). Subsequent observations by the RADAR revealed more than 650 such features, both dry and

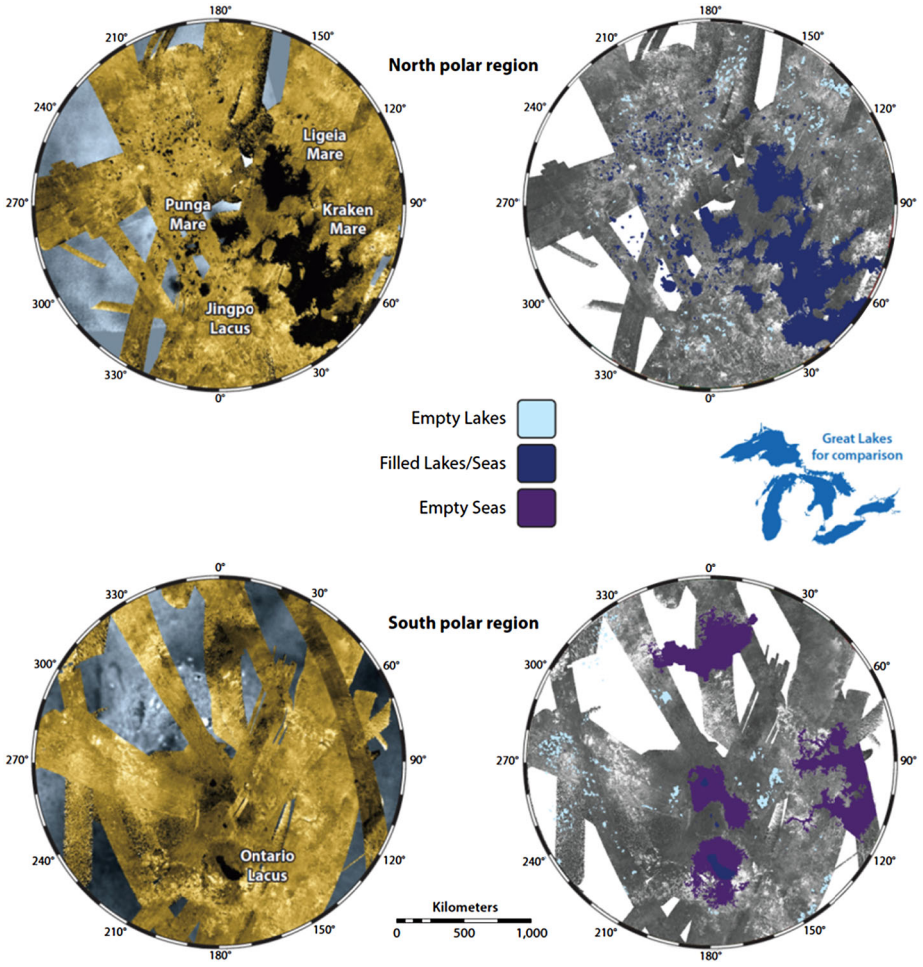

Fig. 17 Map of lakes and seas on the northern (top) and southern (bottom) polar regions of Titan

filled, scattered throughout Titan's polar terrain (Hayes et al. 2008; Birch et al. 2017). These features have diameters that follow a log-normal distribution with a median of 77 ± 20 km (Hayes 2016). The morphology of both dry and filled lakes and seas on Titan provides a record of past and current climatic conditions and surface evolution processes. For example, while Titan's large seas have complex shorelines that are consistent with drowning pre-existing topography, most of the smaller lakes are steep-sided depressions that are more consistent with dissolution-based erosion driven by karstic processes (Hayes et al. 2017; Cartwright et al. 2011; Langhans et al. 2012). For a recent and more detailed review of Cassini's exploration of Titan's lakes and seas, see Hayes (2016).

Lakes and seas encompass 1% of Titan's total surface area (Hayes 2016). The majority of surface liquids (97% by area) reside in the north polar region, with 80% of all liquid-filled surface area contained in three large seas; Kraken Mare, Ligeia Mare, and Punga Mare (Fig. 17). The largest modern liquid body in the south polar region is Ontario Lacus, although several large empty basins that encompass an area similar to the northern Maria

(7.6×10^5 km^2) have been identified and interpreted as paleoseas (Hayes et al. 2010, 2011; Birch et al. 2018). The observed dichotomy in lake distribution has been attributed to a net transport of $\sim 5 \times 10^{14}$ kg of methane per Titan year from the south pole to the north, driven by a seasonal asymmetry in insolation that is the result of Saturn's eccentric orbit around the Sun (Aharonson et al. 2009; Lora and Mitchell 2015). Summer solstice in Titan's southern hemisphere occurs near perihelion while northern summer solstice occurs at aphelion, resulting in 25% higher peak insolation during southern summer as compared to northern summer. Long timescale ($\sim$ 100000 yr) orbital cycles can switch the direction and magnitude of the seasonal asymmetry driving this transport, moving liquid deposits between the poles similar to the way Croll-Milankovitch cycles drive ice ages and other long-term climate effects on Earth (Aharonson et al. 2009). The presence of drowned river valleys at the terminus of channels flowing into the northern seas (Stofan et al. 2006), as well as the presence of exposed and abandoned river deltas adjacent to the shores of southern Ontario Lacus (Wall et al. 2010) support the theory of rising and falling liquid levels as the magnitude and direction of net pole-to-pole methane transport varies with Titan's orbital cycles (Lora et al. 2014).

While a few small lakes have been observed to disappear or brighten in both the north and south over the thirteen years of Cassini observations, no large-scale changes in the sea shorelines have been observed over the course of the mission. Given the resolution of the RADAR and the lack of comparable repeated SAR images, however, this is not surprising. Although confirmed and stable liquid deposits are currently restricted to polar terrain, the equatorial features Hotei and Tui Regiones have been interpreted as possible low-latitude paleoseas (Moore et al. 2014). Both regions are surrounded by fluvial networks that appear to converge on a field of radar-bright, lobate, depressions that are morphologically similar to high-latitude lakes (Moore et al. 2014). Dark flow-like features identified adjacent to the radar-bright depressions have been interpreted as cryovolcanic deposits (Barnes et al. 2006; Wall et al. 2009), suggesting that both paleo-lakes and cryovolcanic flows may be present at Tui Regio and Hotei Regio (Lopes et al. 2013b). The existence of modern equatorial lakes has been proposed based on the longevity of low albedo localities observed by Cassini VIMS (Griffith et al. 2012; Vixie et al. 2015), although none of these features have been observed in higher-resolution SAR or altimetry datasets of the regions. Ample evidence exists (e.g. at the Huygens landing site) for at least transient liquids at low latitudes, and very flat areas exist which may be lake beds. Indeed, strong specular reflections were observed at low latitude by the Arecibo radar on Earth (the longest-range radar astronomy experiment conducted to date) before Cassini's arrival, and the favored interpretation at the time was as extant bodies of smooth liquid hydrocarbons (Campbell et al. 2003).

In May 2014, the RADAR acquired nadir-pointed altimetry over the Ligeia Mare. The resulting altimetry echoes revealed waveforms that displayed two distinct returns, one from the surface of Ligeia Mare and one from its seabed (Mastrogiuseppe et al. 2014). The difference in the received timing between these returns was a direct measure of Ligeia's depth (Fig. 18), while the relative intensity difference between the surface and subsurface return was a measurement of the liquid's loss-tangent (i.e., absorbance). While several studies (e.g., Brown et al. 2008; Lorenz et al. 2008a; Lunine and Lorenz 2009; Cordier et al. 2012; Cornet et al. 2012; Ventura et al. 2012) have used indirect measurements to constrain the depth of Titan's lakes and seas, the altimetry observations over Ligeia represent the first direct measurement of extraterrestrial bathymetry profiles. Following the identification of Ligeia Mare's seabed, several passes of Titan were modified to repeat the experiment over Punga Mare and Kraken Mare (Mastrogiuseppe et al. 2016). A reprocessing of altimetry

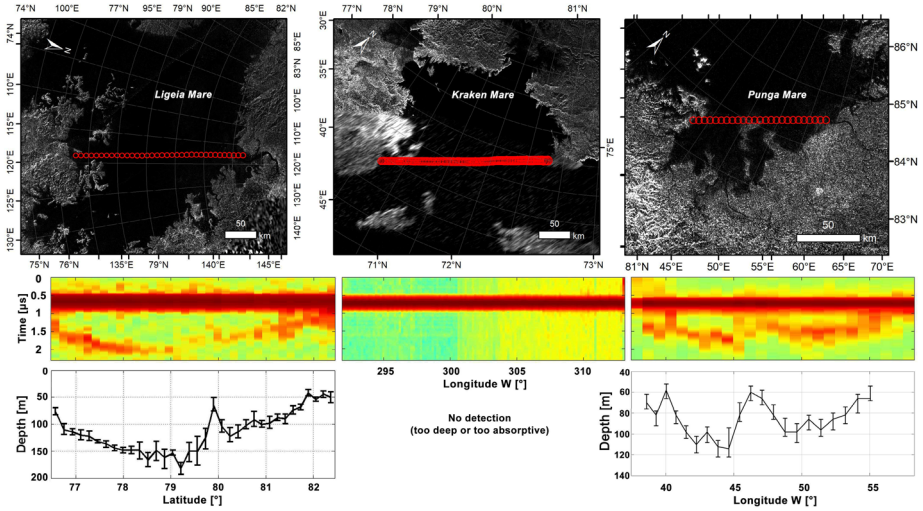

Fig. 18 SAR mosaics, radargrams and relative bathymetries (respectively in the upper, middle and bottom panels) relative to the flyby T91 over Ligeia Mare (left), the flyby T104 over Kraken Mare (center), and the flyby T108 over Punga Mare (right) altimetry observations. Note that seafloor echoes have been detected for Ligeia and Punga Maria, while only surface returns are present over the open sea of Kraken mare

data acquired over Ontario Lacus in December 2008 allowed the technique to be applied to Ontario Lacus as well (Mastrogiuseppe et al. 2018). Ligeia Mare was determined to have a depth of 170 m at the deepest point along the observed track (Mastrogiuseppe et al. 2014) and in combination with SAR images, the total volume of the basins was found to be around ~ 14000 km^3 of liquid (Hayes 2016). The estimated Ku-band loss tangent was $4.4 \pm 1 \times 10^{-5}$ (Mastrogiuseppe et al. 2016). Assuming a methane-ethane-nitrogen composition and using the laboratory measurements of Mitchell et al. (2015) with the Lorentz-Lorenz formulation, the best-fit loss tangent is consistent with a methane-dominated composition of 71% CH_4: 12% C_2H_6: 17% N_2. As large quantities of liquid ethane should have been produced by photolysis of methane in the upper atmosphere, and at least trace amounts of ethane have been detected in Ontario Lacus (Brown et al. 2008), the lack of significant ethane (and other higher order hydrocarbons such as propane) in Titan's lakes and seas requires that the ethane is sequestered in reservoirs (e.g., subsurface liquid deposits or sequestration in crustal clathrate hydrate).

To within error, the loss tangents of Punga Mare and the shallower parts of Kraken Mare (Fig. 18) suggested a composition similar to Ligeia (Mastrogiuseppe et al. 2018). Along most of Kraken Mare the seafloor was not detected, indicating that the seas are either too deep or too absorptive in these areas. Within Punga Mare, a clear detection of the subsurface was observed to reach a maximum depth of up 120 m, along tens of km of track (Mastrogiuseppe et al. 2018). At Ontario Lacus, however, the best fit loss tangent is greater ($7 \pm 3 \times 10^{-5}$), consistent with a composition of $\sim 47\%$ CH_4, $\sim 40\%$ C_2H_6, and $\sim 13\%$ N_2, possibly suggesting an increased abundance of high-order hydrocarbons as compared to the northern seas. This higher loss tangent could be related to an increased abundance of more involatile hydrocarbons and/or nitriles or suspended particulates that represent a lag deposit generated as methane is transported from the south to the north over multiple seasonal cycles. The final radar observation of the bathymetry campaign was the T126 (22 April 2017) final fly-by at Titan. The Cassini RADAR observed several small-medium size (10–50 km)

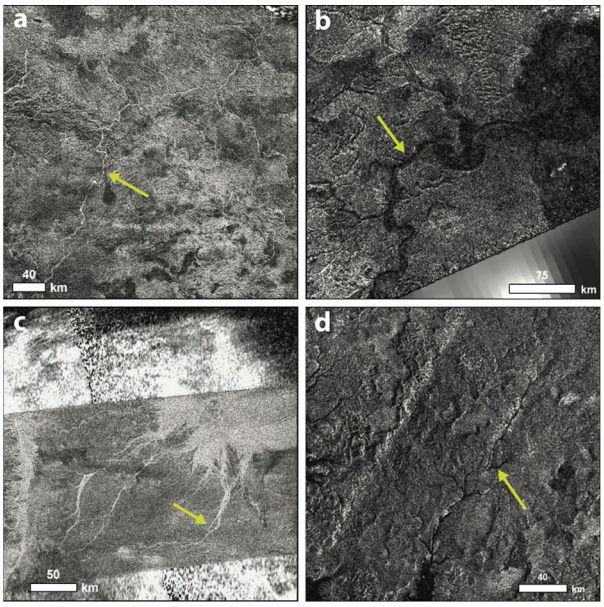

Fig. 19 (**a**) Rectilinear networks in eastern Xanadu; (**b**) Celadon Flumina, a meandering network near the south pole; (**c**) Elvigar Flumina, a braided network that deposits into an alluvial fan; (**d**) Vid Flumina, a dendritic canyon network up to 500 m deep that drains into Ligeia Mare

hydrocarbons lakes present at the northern polar terrain, revealing that such lakes can exceed one hundred meters of depth and have similar loss tangents, and therefore composition, to the northern seas. When the bathymetry measurements are used to anchor models of sea and lake depth from SAR images, the estimated volume of all Titan's observed lakes and seas is $\sim 70000\ km^3$ (Hayes 2016). It is interesting to note that this represents only 1/7 the amount of methane that currently resides in Titan's atmosphere, suggesting that the lakes and seas do not drive global-scale heat transport or meteorology. It is also worthwhile mentioning that measuring the bathymetry and microwave absorptivity of Titan's seas was not planned initially and represents an exciting discovery made during the Cassini spacecraft lifetime.

5.10 Rivers/Channels

When water falls to the surface of the Earth, the most visible conduits on its journey downslope are networks of fluvial channels that slowly transport it toward the oceans. These networks take on many different forms that are the result of the mechanical and chemical properties of the surface (Burr et al. 2006), the climate and weather that generate fluid flow, and the mechanisms that produce topographic relief (Black et al. 2017). The observation of channels on Titan by Cassini and Huygens (Collins 2005; Lorenz et al. 2008c; Lunine et al. 2008; Burr et al. 2009; Black et al. 2012; Burr et al. 2013) has thus provided similar constraints on the nature of Titan's surface and the climatic conditions that proved favorable for the formation of these features, albeit in a far more limited fashion.

Cassini's RADAR imaged large portions of Titan and showed that valley networks are distributed at all latitudes (Lorenz et al. 2008c; Burr et al. 2009; Lopes et al. 2010) and have a wide variety of surface morphologies (Fig. 19). With a diversity of valley networks analogous to the Earth, Cassini has observed canyon networks at the poles (Poggiali et al. 2016), both dendritic and rectilinear networks globally (Burr et al. 2013), and even a meandering-like feature in the south polar region (Malaska et al. 2011b;

Birch et al. 2018). The presence of canyons implies a vertically weak bedrock, which may be influenced by fractures in the ice shell and/or a relatively highly erodible material. Similarly, rectilinear channels imply a fractured bedrock, where channels are forced to follow tectonically-controlled paths of weakness. Meandering networks, meanwhile, imply the presence of a cohesive substrate (Howard et al. 2009). A critical unknown following the Cassini mission, however, is whether there are any systematic variations in morphologic type that may be indicative of crustal heterogeneities (Burr et al. 2013) and/or variations in transport efficiencies/climate change (Moore et al. 2014).

Due to the coarse resolution of the Cassini RADAR, we have been limited to studying only the largest valley networks on Titan. We therefore have a limited idea about the extent to which Titan's landscapes are dissected by fluvial networks. The one exception to this is the region where the Huygens lander descended, where descent images, with an order-of-magnitude higher resolution (Tomasko et al. 2005), showed a highly-dissected network of dendritic valleys (Perron et al. 2006). It is likely that Titan is dissected everywhere at the scale observed by Huygens, however, a definitive answer to this question requires image data and topography with a resolution finer than the scale of fluvial dissection (10's of meters).

While not surprising that Titan has a global network of fluvial valleys, the mere presence of channelized flow conduits implies that the surface material can be eroded either physically or chemically, and that flows of sufficient magnitude, either from precipitation or groundwater, are able to erode Titan's surface. However, using estimates for the initial topography and erodibility of the substrate, channels may be very inefficient agents of erosion on Titan (Black et al. 2012) or there may be a gravel lag deposit that inhibits erosion under Titan's current climate (Howard et al. 2016). Better estimates for the physical and chemical properties of both the bedrock and the fluid(s) (Burr et al. 2006; Cordier et al. 2017; Malaska et al. 2017b; Richardson et al. 2018) are needed to provide better understanding about the role that fluvial channels have played in sculpting Titan's surface.

In some locations, fluvial channels terminate in alluvial or fluvial fans, distributary landforms that indicate a transition from a high to a low elevation (Radebaugh et al. 2016; Birch et al. 2017). These are fairly low in slope, and in some cases can run out to large distances, indicating the carrying power by methane fluid of organic sedimentary rock (Radebaugh et al. 2016). These landforms are widely distributed across the surface, but they are not abundant (Birch et al. 2017). This may indicate there is not frequent rainfall that can generate surface erosion, or that topographic gradients are gentle on a global scale such that these landforms are not readily generated.

6 Temporal Change

Temporal changes were detected on Titan during the course of the Cassini mission, due to seasonal or other effects. Data from more than one instrument are key for determining the possible causes of change. For example, as mentioned in Sect. 5.6, the radiative transfer code analysis of VIMS data from Tui Regio (2005–2009) and Sotra Patera (2005–2006) showed temporal surface albedo changes in two areas identified by SAR as cryovolcanic candidates: Tui Regio darkened by 50% and Sotra Patera brightened by a factor of 2 (Solomonidou et al. 2016). These changes could be due to endogenic, possibly cryovolcanism or degassing, or else meteorological or atmospheric processes, such as atmospheric deposition.

6.1 "Magic Islands"

For the majority of the Cassini Mission, Titan's lakes and seas were observed to be quiescent, with no temporal changes and maximum vertical surface roughness on the order

of millimeters (Barnes et al. 2011b; Stephan et al. 2010; Wye et al. 2009; Zebker et al. 2014; Grima et al. 2017). This lack of observable surface roughness has been attributed to a seasonal effect in which polar winds were too weak to create waves or other dynamic features (Hayes et al. 2013). As the northern hemisphere transitioned from spring equinox to summer solstice, temporal changes were observed in all three of Titan's seas. Specular reflections offset from the geometric specular point were observed by VIMS in Punga Mare (Barnes et al. 2014), transient bright features were observed by RADAR in Ligeia Mare (Hofgartner et al. 2014, 2016) and both offset specular reflections and transient radar bright features were observed in Kraken Mare (Hayes 2016).

The transient bright features were nicknamed "Magic Islands" due to their appearing/disappearing act and similarity in appearance to islands in SAR images. The features are not islands, however, and are most consistent with waves, or floating and/or suspended solids and bubbles. Based on the frequency of these phenomena in analogous terrestrial settings, surface waves (intended to mean roughness of the liquid surface regardless of the process causing the roughness) are the most probable hypothesis. Tides, changes of sea level and changes of the seafloor are unlikely to be the primary cause of the temporal changes. The wave properties (e.g., height, wavelength, and driving wind speed) cannot be uniquely determined from the Magic Island observations alone. Surface roughness on scales of approximately 1 cm or greater would be sufficient to cause the observed brightening. A model for waves on Ligeia Mare suggests that for the expected maximum wind speeds of 1 m/s, a significant wave height of 0.2 m and wavelength of 4 m can be expected (Lorenz and Hayes 2012). Magic Islands were observed in three regions; two in Ligeia Mare (Hofgartner et al. 2014, 2016) and one in Kraken Mare (Hayes 2016).

Figure 20 shows the time evolution of the first and most observed Magic Island region. This region was observed to have "Magic Islands" on two occasions; the transient bright features were in the same location on both occasions but differed in areal extent and morphology. HiSAR and VIMS observations acquired between the two SAR detections did not detect Magic Islands, however, the possibility that the "Magic Islands" were present but not detected in these observations could not be ruled out. "Magic Islands" were definitely not present in SAR observations before the first appearance and after the second appearance (Fig. 20 only includes a subset of the images of the region).

The Kraken "Magic Island" was also observed as a five-micron sunglint by VIMS within two hours after the radar detection. The co-detection of the Kraken Magic Island by both RADAR and VIMS suggests that it is likely caused by surface waves, as the reflecting facets must be smooth at both microwave and micron length scales (Hayes 2016).

6.2 Arrakis Planitia Precipitation and Other Transient Events

The first Cassini observations of surface change on Titan were obtained over Arrakis Planitia, near the south pole, where ISS observed the appearance of dark splotches (interpreted as ponded hydrocarbon liquid) in June 2005 that were not present in the previous observation acquired in July 2004 (Turtle et al. 2009). In October 2004, between those two observations, a large cloud outburst was observed near Titan's South Pole from Earth-based telescopes (Schaller et al. 2006). SAR images and SAR-Topo later found that the ISS dark splotches occurred in topographic depressions that are morphologically similar to steep-sided depressions interpreted as empty lakes in the north (Soderblom et al. 2016). VIMS observations of this area acquired between 2007 and 2009 show that the dark splotches had become brighter than the surrounding terrain (Soderblom et al. 2016). SAR images of the area obtained in October 2007 and December 2008 showed the absence of dark splotches in the

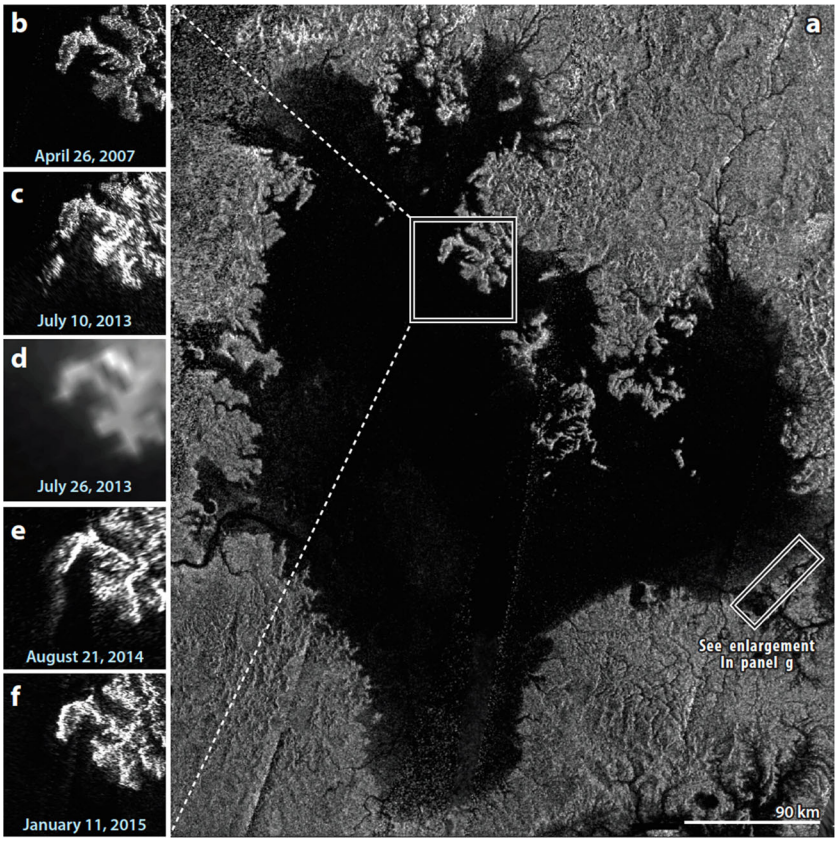

Fig. 20 The large panel on the right is a SAR mosaic of Titan's hydrocarbon sea, Ligeia Mare. The panels on the left show the temporal variation of a region observed to have Magic Islands. Transient bright features (Magic Islands) are observed in the images from July 10, 2013 and August 21, 2014 that are not present in any other images of this region. The VIMS observation on July 26, 2013 (panel **d**) did not detect Magic Islands, however, the possibility that they were present but not detected in these observations could not be ruled out. Magic Islands were definitely not present in SAR observations before the first appearance and after the second appearance. The figure shows only a subset of Cassini observations of the region, see Hofgartner et al. (2016) for all observations with a resolution sufficient to observe the Magic Islands. Figure from Hayes (2016)

same topographic depressions, this time in the microwave, that were interpreted as either the evaporation or infiltration of ponded liquid (Hayes et al. 2011).

In addition to Arrakis Planitia, temporal changes have also been observed at other locations in the south pole as well as within the northern lakes and seas and at equatorial latitudes. The largest observed surface change occurred in 2010 when an equatorial area of over 500000 km in size was observed to darken, presumably by methane precipitation, after a chevron shaped cloud pass over the region (Turtle et al. 2011a). SAR images of the area suggest that the darkened region represented local topographic lows. Showing a similar pattern to the changes observed at Arrakis Planatia, the area was later observed to brighten relative to surrounding terrain and then return to its original albedo (Barnes et al. 2013).

Whereas there have been no definitive changes observed in the shorelines of the northern lakes and seas through April 2017 (flyby T126), there have been several surface changes

reported for lacustrine features in the south polar region. Turtle et al. (2011b) argued for shoreline recession at Ontario Lacus between ISS images acquired June 2005 and March 2009), although the poor resolution of T51 makes quantitative measures difficult. Hayes et al. (2011) found that, while inter-instrument comparisons can be dangerous, SAR images acquired in 2009 (T57/T58) and 2010 (T65) were consistent with a receded shoreline when compared to the June 2005 images obtained by ISS. However, Cornet et al. (2012) argued that, to within measurement error, the data are consistent with no changes at all. Hayes et al. (2011) also discussed repeat RADAR passes of the south acquired in 2007 and 2008/2009 that contain lacustrine features that seem to disappear between subsequent SAR observations. The observed 10-fold increase in SAR backscatter cannot easily be explained by geometric effects and suggests that, between the observations, liquid either infiltrated into the ground, evaporated, or did both (Hayes et al. 2011). Other temporal changes, including roughening events interpreted as wave or fluvial activity as well as Titan's mysterious "magic islands" have been observed within the northern seas. These changes are discussed above in Sect. 6.1.

Although the Cassini mission's exploration of Titan's methane cycles has ended, ground-based observations can continue to monitor Titan's weather until future missions can map fluvial features at a higher resolution and characterize the composition of surface material (including the lakes and seas) through in-situ exploration.

6.3 Observation of a Summer Lag in the North Pole (by Radiometry)

One of the main scientific objectives of the Cassini extended mission (2008–2017) was to monitor the changing seasons on Titan. If any change were to occur, it should be primarily in Titan's polar regions where the most important temperature variations are expected (though limited to 2–4 K over the course of a year).

On board Cassini, both CIRS and the microwave radiometer had the ability to measure the variations of surface/near-surface temperature with time (Jennings et al. 2009; Cottini et al. 2012; Janssen et al. 2016) and both instruments observed a lag in the summer warming of the northern polar terrains (Jennings et al. 2016; Le Gall et al. 2016). They reported a much slower rise of temperature in late spring (2014–2015) than predicted by GCMs, even assuming a very high thermal inertia for lakes and seas (Tokano 2005). Further, there seems to be no significant temperature difference between the land and the seas which suggests that the solid surface surroundings the lakes and seas are saturated with liquid and behave thermally like the liquids. They may as well experience evaporative cooling which would explain the low measured temperatures in the north polar region and have important implication for the hydrocarbon cycle on Titan.

7 Surface and Atmosphere Interaction

7.1 Winds and Temperature

In contrast to the contemporary instantaneous winds revealed by sea surface roughness (see Sect. 6.1), the widespread observations of dunes on Titan attest to winds that have acted over significant periods in the past, and indeed the possibility that aeolian landforms might shed light on Titan's climate history was recognized before Cassini's launch (e.g. Lorenz et al. 1995). Since so few trackable cloud features have been observed on Titan, the aeolian features in Titan's landscape have emerged as one of the principal constraints on Titan's

meteorology. Specifically, it has been estimated that the saltation threshold for the movement of dry sediment on Titan requires surface winds of the order of 1 m/s (e.g. Greeley and Iversen 1987; Lorenz et al. 1995; Lorenz 2014). This estimate is based on an assumption that interparticle cohesion is not too different from terrestrial sands: some laboratory measurements suggest they could be slightly larger (Burr et al. 2015) and it is possible or even likely that (methane/ethane) moisture (Yu et al. 2017) and/or electrostatic charging (Lorenz 2014; Méndez-Harper et al. 2017) could be responsible for stronger cohesion. In any case, the presence of dunes requires winds sometimes exceeding this threshold in the past.

The construction or reorientation time for dunes of the size ($\sim$ 100 m tall) observed by Cassini is substantial, of the order of 50000 years (Ewing et al. 2015; see also Lorenz et al. 1995; Lorenz 2014) and thus not only does the presence of dunes require that the winds have been above the saltation threshold for a substantial integrated period, but also that the dune pattern observed today retains some memory of winds extending into the past by a substantial part or multiple of an astronomical (Croll-Milankovitch) climate cycle (see e.g. Aharonson et al. 2009; Lora et al. 2014). In particular, Ewing et al. (2015) noted that some of Titan's dunes are somewhat crescentic, implying a recent dominance of a northward meridional component to the winds (see also McDonald et al. 2016).

The generally-eastwards direction of sand transport implied by the dune morphology was noted early (Lorenz et al. 2006; Radebaugh et al. 2008; Lorenz and Radebaugh 2009) and was a challenge to meteorological expectations, since low-latitude near-surface winds should have on average an easterly (westwards) flow, much like the trade winds on Earth. Tokano (2008) made some of the first systematic experiments with a global circulation model (GCM) to attempt to reproduce the observed pattern by positing the influence of Xanadu as a highland or bright region. The vexing paradox (see e.g. Lorenz and Zimbelman 2014) was resolved by invoking occasional westward gusts (Tokano 2010; Charnay et al. 2015) such that even though the average wind direction is eastwards, these typical winds are below the threshold speed and so are not reflected in the sand transport. Thus, the landscape is shaped only by the stronger (westward) gusts—with the saltation threshold acting like a 'diode' in an electrical analogy of alternating winds. Tokano (2010) found that a threshold of order 1 m/s was consistent with obtaining a dune pattern similar to that observed and suggested that stronger vertical mixing in the low-latitude troposphere during the equinox period might cause the required westward flows. This idea has been developed somewhat further by Charnay et al. (2015) who suggested that methane rainstorms in particular may be responsible.

Significant developments in the mapping of dune morphology and orientation to wind diversity and sand supply/mobility have taken place in the last decade and a half, stimulated in no small part by the Cassini discovery of large linear dunes as well as other wind-borne features (Lorenz and Radebaugh 2009; Malaska et al. 2016a). Detailed observations suggest that there is a divergence of material transport in the equatorial regions, and a convergence in the mid-latitude regions around latitude 35°. This suggests a relationship exists between two major land units on Titan: the longitudinal dunes and the undifferentiated plains, as discussed in Sect. 5.2. It has been suggested (Rubin and Hesp 2009) that "sticky" sand may yield longitudinal features, and laboratory results with organic material have shown that electrostatic charging may be significant for Titan organics under cryogenic, dry conditions (Méndez-Harper et al. 2017). Nonetheless, the interaction of multiple modes of dune growth may be important in decoding Titan's winds from dunes (e.g. Lucas et al. 2014).

In contrast to the complex wind story, the overall distribution of dunes on Titan is somewhat straightforward from the standpoint of wetness. Early Titan GCM studies (e.g. Rannou et al. 2006; Mitchell 2008) indicated that Titan's low latitudes should be dried out by

the general circulation, as a result of the meridional (Hadley) cells on this slowly rotating world. Thus, the dunes form a broad equatorial belt on Titan, whereas they form belts at about 20 degrees north or south on the faster-rotating Earth. The size and spacing of dunes, assuming that they have been allowed to grow to their full extent without being limited by growth time or sand supply, has been determined (e.g. Andreotti et al. 2009) to correlate to the thickness of the atmospheric boundary layer. Essentially, the layer caps the dune growth once the spacing is roughly equal to the layer thickness. Lorenz et al. (2010) showed that the Huygens descent data was consistent with a boundary layer thickness of the order of 3 km, matching the typical dune spacing on Titan. Extensive dune spacing measurements (e.g. Le Gall et al. 2011; Savage et al. 2014) show only minimal variations with latitude. Charnay and Lebonnois (2012) found that a GCM with an improved boundary layer scheme reproduced the 3 km thickness, interpreting this as a "seasonal" boundary layer.

The full meteorological interpretation of the dune pattern revealed by Cassini's RADAR will require a finer scale of modeling than has been performed so far, including regional topography and albedo effects. It may be that the dune fields, by virtue of having a low thermal inertia and albedo, cause their own "sea breeze" effect, modifying the local winds. The role of evolving ground moisture remains to be elucidated, although some hints of moisture effects on ground thermal inertia have been suggested in the RADAR radiometry data (Janssen et al. 2016).

Although the radiometer in principle is an indicator of surface temperature and could be used to independently constrain gradients with latitude etc. (e.g. Lorenz et al. 2003), in practice the surface temperature estimates from the Cassini Composite Infrared Spectrometer (CIRS) and the Huygens probe have been adopted as "ground truth" and the interpretation of the microwave radiometry has been principally in terms of the surface dielectric properties. However, future studies might profitably examine small-scale radiometer variations and their correlation with surface elevation—in principle the $\sim$ 1 K/km lapse rate may have a signature in surface brightness temperature.

7.2 Methanologic Cycle

Titan is the only place in the solar system, other than Earth, that is known to have an active hydrologic cycle. Titan's methane-based hydrologic cycle is an extreme analog to Earth's water cycle. Exchange processes between atmospheric, surface, and subsurface reservoirs produce methane and ethane cloud systems, as well as erosional and depositional landscapes that have strikingly similar forms to their terrestrial counterparts. Over its thirteen-year exploration of the Saturn system, Cassini has revealed that Titan's hydrocarbon-based hydrology is driven by nested methane cycles that operate over a range of timescales including geologic, orbital, seasonal, and that of a single convective storm. A fast physical (phase change) cycle drives active weather and fluvial processes over seasonal to orbital timescales. A medium-paced chemical cycle siphons off methane for photochemical synthesis in the upper atmosphere, depositing the products on the surface over timescales of millions of years. A long-term geologic cycle may sporadically inject methane into the system from Titan's interior over the age of the solar system. For a recent review of Titan's hydrologic cycle, see Hayes et al. (2018).

8 Titan as a System

Titan is the only moon in the solar system with an atmosphere so massive that it dominates the total volatile inventory in the surface-atmosphere system as well as providing strong

radiative forcing and an active meteorology (Lorenz et al. 2005). It also obscures the surface from view in both the optical and infrared, which is why the Cassini RADAR has been such a crucial tool. However, by the irreversible deposition of heavy hydrocarbons, nitriles, and other photochemical products from methane and nitrogen, the atmosphere also obscures the underlying surface geology to some extent. Were the current inventory of methane to condense onto the surface, it would form a layer 5 meters thick (Mitchell and Lora 2016), but a variety of evidence suggests that many times that number is present in various solid and liquid deposits of organics on and within the ice shell (Hayes et al. 2018).

Therefore, Titan's geologic history is poorly constrained and in particular there is a significant uncertainty as to what fraction of the body's 4.5 billion years of existence is recorded on the surface. Observations relevant to its history include:

(1) The low observed numbers of impact craters (Porco et al. 2005) yield an age of hundreds of millions of years, not billions (Lorenz et al. 2007; Wood et al. 2010; Neish and Lorenz 2012).
(2) The rate of photodissociation of methane in Titan's atmosphere implies that the current gaseous inventory will be depleted in some tens of millions of years (Yung et al. 1984).
(3) Titan's interior has at least partially differentiated, resulting in a rock-metal deep interior, a high-pressure ice layer of uncertain thickness, a liquid water ocean (Iess et al. 2010) perhaps with salts and ammonia (Mitri et al. 2014), and an ice shell 50 to 150 km thick. The deep interior is either significantly hydrated (Castillo-Rogez and Lunine 2010), or there is a mixed rock-ice layer somewhere in the interior (see, e.g., Tobie et al. 2014).
(4) A range of chemical and physical data from the atmosphere to the interior suggest that a significant event, or change in the way Titan evolves, occurred sometime between a few hundred million and a billion years ago (Hörst 2017).

The relatively youthful age of the surface, which may be the result of geologic activity, older impacts occurring on surfaces covered by liquids (Neish and Lorenz 2014), extensive erosion, or substantial burial in organic matter, means that there is little if any geologic evidence of the first 3/4 of Titan's history. Two unanswered questions are (1) what was the process/processes that eroded or covered older impact craters and other landforms, and (2) did the obscuration of features older than a few hundred million years occur continuously over time, or in some singular event?

There is no evidence to answer the second question, but a theoretical model of the evolution of Titan's interior by Tobie et al. (2006) provides an intriguing scenario that implies Titan had a significant change in the working of its interior, ice shell, and atmosphere about 500 million years ago (Wood 2018). In the Tobie et al. (2006) model, Titan had a thin and rigid clathrate ice shell—with methane as the dominant guest species—up until 500 million to one billion years ago. During that earlier epoch, several major heating events resulted in the release of large (compared to the present atmospheric inventory) amounts of methane from the clathrate hydrate into the surface-atmosphere system. Within the last 500–1000 million years the interior has cooled sufficiently to allow an ice I shell to form underneath the buoyant clathrate hydrate ice shell, with diapirism in the thickening ice I shell providing one or several episodes of further release of methane into the surface-atmosphere system. Wood (2018) called the onset of the ice I subcrust (ice shell) the "Great Crustal Thickening Event" and noted that the mode of geologic processes would change dramatically as Titan transitioned from a body with a thin rigid conductive ice shell over the ocean to one with a thicker and rheologically heterogenous ice shell.

Models of Titan's interior look broadly similar but with substantial disagreements on the thickness of the high pressure ice layer and the extent of silicate deep interior (core) hydration (Tobie et al. 2014). How much this affects the surface evolution is unclear. While the idea is commonly held that the source of the methane to resupply the atmosphere is in crustal clathrate hydrate (such a crust/ice shell was predicted in pre-Voyager days; Lewis 1971), how the resupply works is unclear. Simple forcing out of the methane from the clathrate by the photochemically produced ethane eventually fails because of the stoichiometry (two methane molecules making one ethane), although this replacement could eventually weigh down the ice shell and cause an overturn because clathrate with predominantly ethane is heavier than Ice I. (Choukroun and Sotin 2012). This could cause interesting geologic consequences in the present era when the clathrate is nominally underlain by warm ice I. Whether the methane hydrological cycle that we see today shaping so many aspects of Titan's surface is ancient or recent, episodic (Lunine et al. 1998) or continuous, remains a mystery that may be directly coupled to the poorly understood interior evolution. Or it may reflect a series of external events whose record in the Saturn system has yet to be properly read.

Birch et al. (2017) have pointed to geologic evidence (notably the presence of large sedimentary deposits) suggesting that the present epoch of lakes and seas of methane, ethane and nitrogen might have been preceded by one with a widespread ocean of methane and other hydrocarbons. The longevity of such an ocean, in particular its decline, may be constrained by the limits on tidal dissipation of the orbital eccentricity during ocean shrinkage (Sagan and Dermott 1982; Sears 1995), since we now have a measured global Titan topography. Finally, it is possible that Titan has run out of atmospheric and surface methane multiple times in its history, leading to dramatic atmospheric changes (Lorenz et al. 1997) and possibly epochs in the which the surface is worked by liquid nitrogen seas and rivers (Charnay et al. 2014).

If Titan's geologic and atmospheric nature have changed in a secular way over its history, it would join the "other" terrestrial planets—Venus, Earth, and Mars, in this regard. In each case, interior and surface-atmosphere changes over time have led to present-day characteristics that are likely to have been dramatically different from those in the past.

While major progress on understanding Titan was made by the Cassini mission, the limited opportunities for observations with all Cassini's instruments, not just RADAR, have left many questions for future missions to answer. Cassini was a Saturn orbiter, and Titan flybys were limited and brief. Only about half of Titan's surface was mapped with SAR, and coverage in the near-infrared was similarly limited by observation time and spatial resolution. The outstanding questions after the Cassini-Huygens mission were discussed by Nixon et al. (2018) as Titan's "cold case files". Among these are some related to topics discussed in this paper, such as the age of Titan's surface, the thickness of the ice shell, the depth of the interior ocean, whether cryovolcanic features are present and whether cryovolcanism is still occurring, the composition of the surface, whether there are or were lakes at mid-latitudes, what is the variability of composition between the lakes and seas, and where lakes and seas existed in the past. Titan after Cassini has also become a key world in which to study astrobiology and to investigate what complex chemistry, and possible biological activity, may be happening in its surface and subsurface ocean.

Acknowledgements We thank Robert M. Nelson and an anonymous reviewer for excellent and detailed reviews that greatly improved the manuscript, and Phil Callahan for an informal review and helpful suggestions for improvement. Part of this work was carried out at the Jet Propulsion Laboratory, California Institute of technology, under contract with NASA. Copyright 2018, California Institute of Technology. Government sponsorship is acknowledged.

References

O. Aharonson, A.G. Hayes, J.I. Lunine, R.D. Lorenz, M.D. Allison, C. Elachi, An asymmetric distribution of lakes on Titan as a possible consequence of orbital forcing. Nat. Geosci. **2**(12), 851 (2009)

B. Andreotti, A. Fourriere, F. Ould-Kaddour, B. Murray, P. Claudin, Giant aeolian dune size determined by the average depth of the atmospheric boundary layer. Nature **457**(7233), 1120 (2009)

N. Artemieva, J.I. Lunine, Numerical calculations of the longevity of impact oases on Titan. Icarus **173**, 243–253 (2005)

J.W. Barnes, R.H. Brown, E.P. Turtle, A.S. McEwen, R.D. Lorenz, M. Janssen, E.L. Schaller, M.E. Brown, B.J. Buratti, C. Sotin, C. Griffith, R. Clark, J. Perry, S. Fussner, J. Barbara, R. West, C. Elachi, A.H. Bouchez, H.G. Roe, K.H. Baines, G. Bellucci, J-P. Bibring, F. Capaccioni, P. Cerroni, M. Combes, A. Coradini, D.P. Cruikshank, P. Drossart, V. Formisano, R. Jaumann, Y. Langevin, D.L. Matson, T.B. McCord, P.D. Nicholson, B. Sicardy, A 5-micron-bright spot on Titan: evidence for surface diversity. Science **310**, 92–95 (2005). https://doi.org/10.1126/science.1117075

J.W. Barnes, R.H. Brown, J. Radebaugh, B.J. Buratti, C. Sotin, S. Le Mouelic, S. Rodriguez, E.P. Turtle, J. Perry, R. Clark, K.H. Baines, P.D. Nicholson, Cassini observations of flow-like features in western Tui Regio, Titan. Geophys. Res. Lett. **33**, L16204 (2006). https://doi.org/10.1029/2006GL026843

J. Barnes, J. Radebaugh, R.H. Brown, S. Wall, L. Soderblom, J. Lunine, D. Burr, C. Sotin, S. Le Mouelic, S. Rodriguez, B.J. Buratti, R. Clark, K.H. Baines, R. Jaumann, P.D. Nicholson, R.L. Kirk, R. Lopes, R. Lorenz, K. Mitchell, C.A. Wood, Near-infrared spectral mapping of Titan's mountains and channels. J. Geophys. Res. **112**, E11006 (2007a). https://doi.org/10.1029/2007JE002932

J.W. Barnes, R.H. Brown, L. Soderblom, B.J. Buratti, C. Sotin, S. Rodriguez et al., Global-scale surface spectral variations on Titan seen from Cassini/VIMS. Icarus **186**, 242–258 (2007b)

J.W. Barnes, R.H. Brown, L. Soderblom, C. Sotin, S. Le Mouelic, S. Rodriguez, R. Jaumann, R.A. Beyer, R. Clark, P. Nicholson, Spectroscopy, morphometry, and photoclinometry of Titan's dunefields from Cassini/VIMS. Icarus **195**, 400–414 (2008)

J.W. Barnes, J. Bow, J. Schwartz, R.H. Brown, J.M. Soderblom, A.G. Hayes, G. Vixie, S. Le Mouelic, S. Rodriguez, C. Sotin, R. Jaumann, K. Stephan, L.A. Soderblom, R.N. Clark, B.J. Buratti, K.H. Baines, P.D. Nicholson, Organic sedimentary deposits in Titan's dry lakebeds: probable evaporate. Icarus **216**, 136–140 (2011a)

J.W. Barnes, J.M. Soderblom, R.H. Brown, Wave constraints for Titan's Jingpo Lacus and Kraken Mare from VIMS specular reflection lightcurves. Icarus **211**, 722–731 (2011b). https://doi.org/10.1016/j.icarus.2010.09.022

J.W. Barnes, B.J. Buratti, E.P. Turtle, J. Bow, P.A. Dalba, J. Perry, R.H. Brown, S. Rodriguez, S. Le Mouélic, K.H. Baines, C. Sotin, R.D. Lorenz, M.J. Malaska, T.B. McCord, R.N. Clark, R. Jaumann, P.O. Hayne, P.D. Nicholson, J.M. Soderblom, L.A. Soderblom, Precipitation-induced surface brightenings seen on Titan by Cassini VIMS and ISS. Planet. Sci. **2**, 1 (2013). https://doi.org/10.1186/2191-2521-2-1

J.W. Barnes, C. Sotin, J.M. Soderblom et al., Cassini/VIMS observes rough surfaces on Titan's Punga mare in specular reflection. Planet. Sci. **3**, 17 (2014). https://doi.org/10.1186/s13535-014-0003-4

C. Béghin, O. Randriamboarison, M. Hamelin, E. Karkoschka, C. Sotin, R.C. Whitten, J.-J. Berthelier, R. Grard, F. Simoes, Analytic theory of Titan's Schumann resonance: constraints on ionospheric conductivity and buried water ocean. Icarus **218**, 1028–1042 (2012)

J.-M. Bernard, E. Quirico, O. Brissaud, G. Montagnac, B. Reynard, B.P. McMillan, P. Coll, M.-J. Nguyen, F. Raulin, B. Schmitt, Reflectance spectra and chemical structure of Titan's tholins: application to the analysis of Cassini Huygens observations. Icarus **185**, 301–307 (2006)

B.G. Bills, F. Nimmo, Rotational dynamics and internal structure of Titan. Icarus **214**(1), 351–355 (2011)

S.P.D. Birch, A.G. Hayes, P. Corlies, E.R. Stofan, J.D. Hofgartner, R.M.C. Lopes, R.D. Lorenz, J.I. Lunine, S.M. MacKenzie, M.J. Malaska, C.A. Wood (the Cassini RADAR Team), Morphologic evidence that Titan's southern hemisphere basins are paleoseas. Icarus **310**, 140–148 (2017). https://doi.org/10.1016/j.icarus.2017.12.016

S.P.D. Birch, A.G. Hayes, J.D. Hofgartner, The raised rims of Titan's small lakes, in *49th Lunar and Planetary Science Conference*, 19–23 March, 2018, The Woodlands, Texas. LPI Contribution, vol. 2083 (2018)

B.A. Black, J.T. Perron, D.M. Burr, S.A. Drummond, Estimating erosional exhumation on Titan from drainage network morphology. J. Geophys. Res. **117**, E08006 (2012)

B.A. Black, J.T. Perron, D. Hemingway, E. Bailey, F. Nimmo, H. Zebker, Global drainage patterns and the origins of topographic relief on Earth, Mars, and Titan. Science **356**, 727–731 (2017)

L.E. Bonnefoy, A.G. Hayes, P.O. Hayne, M.J. Malaska, A. Le Gall, A. Solomonidou, A. Lucas, Compositional and spatial variations in Titan dune and interdune regions from Cassini VIMS and RADAR. Icarus **270**, 222–237 (2016)
C. Brassé, O. Munoz, P. Coll, F. Raulin, Optical constants of Titan aerosols and their tholins analogs: experimental results and modeling/observational data. Planet. Space Sci. **109–110**, 159–174 (2015)
R.H. Brown, K.H. Baines, G. Bellucci, J.-P. Bibring, B.J. Buratti, F. Capaccioni et al., The Cassini Visual and Infrared Mapping Spectrometer (VIMS) investigation. Space Sci. Rev. **115**, 111–168 (2004). https://doi.org/10.1007/s11214-004-1453-x
R.H. Brown, L.A. Soderblom, J.M. Soderblom, R.N. Clark, R. Jaumann, J.W. Barnes, C. Sotin, B. Buratti, K.H. Baines, P.D. Nicholson, The identification of liquid ethane in Titan's Ontario Lacus. Nature **454**, 607–610 (2008). https://doi.org/10.1038/nature07100
B.J. Buratti, C. Sotin, K. Lawrence, R.H. Brown, S. Le Mouélic, J.M. Soderblom et al., A newly discovered impact crater in Titan's Senkyo Cassini VIMS observations and comparison with other impact features. Planet. Space Sci. **60**, 18–25 (2012)
D.M. Burr, J.P. Emery, R.D. Lorenz, G.C. Collins, P.A. Carling, Sediment transport by liquid surficial flow: application to Titan. Icarus **181**, 235–242 (2006)
D.M. Burr, R.E. Jacobsen, D.L. Roth, C.B. Phillips, K.L. Mitchell, D. Viola, Fluvial network analysis on Titan: evidence for subsurface structures and west-to-east wind flow, southwestern Xanadu. Geophys. Res. Lett. **36**, L22203 (2009)
D.M. Burr, S.A. Drummond, R. Cartwright, B.A. Black, J.T. Perron, Morphology of fluvial networks on Titan: evidence for structural control. Icarus **226**, 742–759 (2013)
D.M. Burr, N.T. Bridges, J.R. Marshall, J.K. Smith, B.R. White, J.P. Emery, Higher-than-predicted saltation threshold wind speeds on Titan. Nature **517**(7532), 60 (2015)
D.B. Campbell, G.J. Black, L.M. Carter, S.J. Ostro, Radar evidence for liquid surfaces on Titan. Science **302**(5644), 431–434 (2003)
R. Cartwright, J.A. Clayton, R.L. Kirk, Channel morphometry, sediment transport, and implications for tectonic activity and surficial ages of Titan basins. Icarus **214**(2), 561–570 (2011)
J.C. Castillo-Rogez, J.I. Lunine, Evolution of Titan's rocky core constrained by Cassini observations. Geophys. Res. Lett. **37**, L20205 (2010). https://doi.org/10.1029/2010GL044398
B. Charnay, S. Lebonnois, Two boundary layers in Titan's lower troposphere inferred from a climate model. Nat. Geosci. **5**(2), 106–109 (2012)
B. Charnay, F. Forget, G. Tobie, C. Sotin, R. Wordsworth, Titan's past and future: 3D modeling of a pure nitrogen atmosphere and geological implications. Icarus **241**, 269–279 (2014)
B. Charnay, E. Barth, S. Rafkin, C. Narteau, S. Lebonnois, S. Rodriguez, S.C. Du Pont, A. Lucas, Methane storms as a driver of Titan's dune orientation. Nat. Geosci. **8**(5), 362 (2015)
M. Choukroun, S. Sotin, Is Titan's shape caused by its meteorology and carbon cycle? Geophys. Res. Lett. **39**, L04201 (2012). https://doi.org/10.1029/2011GL050747
R.N. Clark, J.M. Curchin, J.W. Barnes, R. Jaumann, L. Soderblom, D.P. Cruikshank, R.H. Brown, S. Rodriguez, J. Lunine, K. Stephan, T.M. Hoefen, Detection and mapping of hydrocarbon deposits on Titan. J. Geophys. Res., Planets **115**(E10), E10005 (2010). https://doi.org/10.1029/2009JE003369
G.C. Collins, Relative rates of flucial bedrock incision on Titan and Earth. Geophys. Res. Lett. **32**(22), L22202 (2005)
C. Cook-Hallett, J.W. Barnes, S.A. Kattenhorn, T. Hurford, J. Radebaugh, B. Stiles, M. Beuthe, Global contraction/expansion and polar lithospheric thinning on Titan from patterns of tectonism. J. Geophys. Res., Planets **120**(6), 1220–1236 (2015)
D. Cordier, O. Mousis, J.I. Lunine, P. Lavvas, V. Vuitton, An estimate of the chemical composition of Titan's lakes. Astrophys. J. **707**, L128–L131 (2009). https://doi.org/10.1088/0004-637X/707/2/L128
D. Cordier, O. Mousis, J.I. Lunine, S. Lebonnois, P. Rannou, P. Lavvas, L.Q. Lobo, A.G.M. Ferreira, Titan's lakes chemical composition: sources of uncertainties and variability. Planet. Space Sci. **61**(1), 99–107 (2012)
D. Cordier, F. García-Sánchez, D.N. Justo-García, G. Liger-Belair, Bubble streams in Titan's seas a product of liquid $N_2 + CH_4 + C_2H_6$ cryogenic mixture. Nat. Astron. **1**, 1–4 (2017). https://doi.org/10.1038/s41550-017-0102
P. Corlies et al., Titan's topography and shape at the end of the Cassini mission. Geophys. Res. Lett. **44**(23), 11754–11761 (2017)
T. Cornet, O. Bourgeois, S. Le Mouélic, S. Rodriguez, T. Lopez Gonzalez, C. Sotin, G. Tobie, C. Fleurant, J.W. Barnes, R.H. Brown, Geomorphological significance of Ontario Lacus on Titan: integrated interpretation of Cassini VIMS, ISS and RADAR data and comparison with the Etosha Pan (Namibia). Icarus **218**(2), 788–806 (2012)
T. Cornet, D. Cordier, T. Le Bahers, O. Bourgeois, C. Fleurant, S. Le Mouélic, N. Altobelli, Dissolution on Titan and on Earth: toward the age of Titan's karstic landscapes. J. Geophys. Res., Planets **120**, 1044–1074 (2015). https://doi.org/10.1002/2014JE004738

T. Cornet, C. Fleurant, B. Signovert, D. Cordier, O. Bourgois, S. Le Mouélic, S. Rodriguez, A. Lucas, Landscape formation through dissolution on Titan: a 3D landscape evolution model, in *Lunar and Planetary Science 2017* (2017). Abstract 1835

V. Cottini, C.A. Nixon, D.E. Jennings, R. de Kok, N.A. Teanby, P.G.J. Irwin, F.M. Flasar, Spatial and temporal variations in Titan's surface temperatures from Cassini CIRS observations. Planet. Space Sci. **60**(1), 62–71 (2012). https://doi.org/10.1016/j.pss.2011.03.015

S. Courrech du Pont, C. Narteau, X. Gao, Two modes for dune orientation. Geology (2014). https://doi.org/10.1130/G35657.1

A. Coustenis, E. Lellouch, R. Wittemberg, J.-P. Maillard, C.P. Mckay, Modelling Titan's surface from near-IR FTS/CFHT1995–1996 spectra, in *22nd General Assembly of the European Geophysical Society*, 21–25 April, Vienne (1997)

M.E. Davies, T.R. Colvin, P.G. Rogers, P.W. Chodas, W.L. Sjogren, E.L. Akim, V.A. Stepaniants, Z.P. Vlasova, A.I. Zakharov, The rotation period, direction of the North Pole, and geodetic control network of Venus. J. Geophys. Res. **97**(E8), 13141–13151 (1992)

C. Elachi, M.D. Allison, L. Borganelli, P. Encrenaz, E. Im, M.A. Janssen, W.T.K. Johnson, R.L. Kirk, R.D. Lorenz, J.I. Lunine, D.O. Muhleman, S.J. Ostro, G. Picardi, F. Posa, C.G. Rapley, L.E. Roth, S. Seu, L.A. Soderblom, S. Vetrella, S.D. Wall, C.A. Wood, H.A. Zebker, Radar: The Cassini Titan Radar Mapper. Space Sci. Rev. **115**, 71–110 (2004)

E. Elachi et al., Cassini Radar views the surface of Titan. Science **308**, 970–974 (2005)

R.C. Ewing, A.G. Hayes, A. Lucas, Sand dune patterns on Titan controlled by long-term climate cycles. Nat. Geosci. **8**(1), 15–19 (2015)

S.G. Fryberger, G. Dean, Dune forms and wind regime, in *A Study of Global Sand Seas*, ed. by E.D. McKee. U.S. Geol. Surv. Prof. Pap., vol. 1052 (1979), pp. 137–169

C.R. Glein, E.L. Shock, A geochemical model of non-ideal solutions in the methane-ethane-propane-nitrogen-actylene system on Titan. Geochim. Cosmochim. Acta **115**, 217–240 (2013). https://doi.org/10.1016/j.gca.2013.03.030

R. Greeley, J.D. Iversen, *Wind as a Geological Process: On Earth, Mars, Venus and Titan, vol. 4* (Cambridge University Press, Cambridge, 1987)

C.A. Griffith, L. Doose, M.G. Tomasko, P.F. Penteado, C. See, Radiative transfer analyses of Titan's tropical atmosphere. Icarus **218**(2), 975–988 (2012)

C. Grima, M. Mastrogiuseppe, A.G. Hayes, S.D. Wall, R.D. Lorenz, J.D. Hofgartner, B.C. Stiles, C. Elachi (The Cassini RADAR Team), Surface roughness of Titan's hydrocarbon seas. Earth Planet. Sci. Lett. **474**, 20–24 (2017)

A.G. Hayes, The lakes and seas of Titan. Annu. Rev. Earth Planet. Sci. **44**, 57–83 (2016)

A. Hayes, O. Aharonson, P. Callahan, C. Elachi, Y. Gim, R. Kirk, K. Lewis, R. Lopes, R. Lorenz, J. Lunine et al., Hydrocarbon lakes on Titan: distribution and interaction with a porous regolith. Geophys. Res. Lett. **35**(9), L09204 (2008)

A.G. Hayes, A.S. Wolf, O. Aharonson, H. Zebker, R. Lorenz, R.L. Kirk, P. Paillou, J. Lunine, L. Wye, P. Callahan et al., Bathymetry and absorptivity of Titan's Ontario Lacus. J. Geophys. Res. **115**(E9), E09009 (2010)

A.G. Hayes, O. Aharonson, J.I. Lunine, R.L. Kirk, H.A. Zebker, L.C. Wye, R.D. Lorenz, E.P. Turtle, P. Paillou, G. Mitri et al., Transient surface liquid in Titan's polar regions from Cassini. Icarus **211**(1), 655–671 (2011)

A.G. Hayes, R.D. Lorenz, M.A. Donelan et al., Wind driven capillary-gravity waves on Titan's lakes: hard to detect or non-existent? Icarus **225**, 403–412 (2013). https://doi.org/10.1016/j.icarus.2013.04.004

A.G. Hayes, S.P.D. Birch, W.E. Dietrich, A.D. Howard, R.L. Kirk, V. Poggiali, M. Mastrogiuseppe, R.J. Michaelides, P.M. Corlies, J.M. Moore et al., Topographic constraints on the evolution and connectivity of Titan's lacustrine basins. Geophys. Res. Lett. **44**(23), 11,745–11,753 (2017)

A.G. Hayes, R.D. Lorenz, J.I. Lunine, A post-Cassini view of Titan's methane-based hydrologic cycle. Nat. Geosci. **11**, 306–313 (2018)

D.J. Hemingway, F. Nimmo, H. Zebker, L. Iess, A rigid and weathered ice shell on Titan. Nature **500**, 550–552 (2013)

D.J. Hemingway, L. Iess, R. Tajeddine, G. Tobie, The interior of Enceladus, in *Enceladus and the Icy Moons of Saturn*, ed. by P.M. Schenk, R.N. Clark, C.J.A. Howett, A.J. Verbiscer (University of Arizona Press, Tucson, 2018), pp. 57–77

M. Hirtzig, B. Bézard, E. Lellouch, A. Coustenis, C. de Bergh, P. Drossart, A. Campargue, V. Boudon, V. Tyuterev, P. Rannou, T. Cours, S. Kassi, A. Nikitin, D. Mondelain, S. Rodriguez, S. Le Mouélic, Titan's surface and atmosphere from Cassini/VIMS data with updated methane opacity. Icarus **226**, 470–486 (2013)

J.D. Hofgartner, A.G. Hayes, J.I. Lunine et al., Transient features in a Titan sea. Nat. Geosci. **7**, 493–496 (2014). https://doi.org/10.1038/ngeo2190

J.D. Hofgartner, A.G. Hayes, J.I. Lunine et al., Titan's "Magic Islands": transient features in a hydrocarbon sea. Icarus **271**, 338–349 (2016)

S. Hörst, Titan's atmosphere and climate. J. Geophys. Res., Planets **122**, 432–482 (2017). https://doi.org/10.1002/2016JE005240

M. Howard, S. Bastea, L.E. Fried, B. Khare, C.P. McKay, Titans' interior chemical composition: a thermo chemical assessment, in *American Astronomical Society, DPS Meeting*, vol. 41 (2009)

A.D. Howard, S. Breton, J.M. Moore, Formation of gravel pavements during fluvial erosion as an explanation for persistence of ancient cratered terrain on Titan and Mars. Icarus **270**, 100–113 (2016). https://doi.org/10.1016/j.icarus.2015.05.034

L. Iess et al., Gravity field, shape, and moment of inertia of Titan. Science **327**, 1367 (2010). https://doi.org/10.1126/science.1182583

L. Iess et al., The tides of Titan. Science **337**, 457 (2012). https://doi.org/10.1126/science.1219631

M.A. Janssen, R.D. Lorenz, R. West, F. Paganelli, R.M. Lopes, R.L. Kirk, C. Elachi, S.D. Wall, W.T.K. Johnson, Y. Anderson, R.A. Boehmer, P. Callahan, Y. Gim, G.A. Hamilton, K.D. Kelleher, L. Roth, B. Stiles, A. Le Gall (the Cassini Radar Team), Titan's surface at 2.2-cm wavelength imaged by the Cassini RADAR Radiometer: calibration and first results. Icarus **200**, 222–239 (2009). https://doi.org/10.1016/j.icarus.2008.10.017

M.A. Janssen, A. Le Gall, L.C. Wye, Anomalous radar backscatter from Titan's surface? Icarus **212**(1), 321–328 (2011)

M.A. Janssen, A. Le Gall, R.M. Lopes, R.D. Lorenz, M.J. Malaska, A.G. Hayes, C.D. Neish, A. Solomonidou, K.L. Mitchell, J. Radebaugh, S.J. Keihm, Titan's surface at 2.18-cm wavelength imaged by the Cassini RADAR radiometer: results and interpretations through the first ten years of observation. Icarus **270**, 443–459 (2016)

R. Jaumann, R.H. Brown, K. Stephan, J.W. Barnes, L.A. Soderblom, C. Sotin, S. Le Mouélic, R.N. Clark, J. Soderblom, B.J. Buratti et al., Fluvial erosion and post-erosional processes on Titan. Icarus **197**(2), 526–538 (2008)

D.E. Jennings et al., Titan's surface brightness temperatures. Astrophys. J. **691**, L103–L105 (2009)

D.E. Jennings et al., Surface temperatures on Titan during Northern winter and spring. Astrophys. J. Lett. **816**, L17 (2016)

E. Karkoschka, A. McEwen, J. Perry, *Creating the Best Global Mosaic of Titan's Surface Albedo Using Cassini Images*. AAS/Division for Planetary Sciences Meeting Abstract #49 (2017)

R.L. Kirk, E. Howington-Kraus, A.G. Hayes, R.M.C. Lopes, R.D. Lorenz, J.I. Lunine, K.L. Mitchell, E.R. Stofan, S.D. Wall, La Sotra y los otros: topographic evidence for (and against) cryovolcanism on Titan, in *Eos Trans. AGU, 91(52), Fall Meet. Suppl.* (2010). Abstract P22A-03

D.G. Korycansky, K.J. Zahnle, Modeling crater populations on Venus and Titan. Planet. Space Sci. **53**, 695–710 (2005)

M.H. Langhans, R. Jaumann, K. Stephan, R.H. Brown, B.J. Buratti, R.N. Clark, K.H. Baines, P.D. Nicholson, R.D. Lorenz, L.A. Soderblom et al., Titan's fluvial valleys: morphology, distribution, and spectral properties. Planet. Space Sci. **60**(1), 34–51 (2012)

A. Le Gall, M.A. Janssen, P. Paillou, R.D. Lorenz, S.D. Wall, Radar-bright channels on Titan. Icarus **207**, 948–958 (2010)

A. Le Gall, M.A. Janssen, L.C. Wye, A.G. Hayes, J. Radebaugh, C. Savage, H. Zebker, R.D. Lorenz, J.I. Lunine, R.L. Kirk, R.M.C. Lopes, S. Wall, P. Callahan, E.R. Stofan, T. Farr (the Cassini Radar Team), Cassini SAR, radiometry, scatterometry and altimetry observations of Titan's dune fields. Icarus **213**, 608–624 (2011)

A. Le Gall, A.G. Hayes, R. Ewing, M.A. Janssen, J. Radebaugh, C. Savage, P. Encrenaz (the Cassini Radar Team), Latitudinal and altitudinal controls on Titan's dune field morphometry. Icarus **217**, 231–242 (2012)

A. Le Gall, M.J. Malaska, R.D. Lorenz, M.A. Janssen, T. Tokano, A.G. Hayes, M. Mastrogiuseppe, J.I. Lunine, G. Veyssière, P. Encrenaz, O. Karatekin, Composition, seasonal change and bathymetry of Ligeia Mare, Titan, derived from its microwave thermal emission. J. Geophys. Res., Planets **121**, 233–251 (2016)

S. Le Mouelic, P. Paillou, M.A. Janssen, J.W. Barnes, S. Rodriguez, C. Sotin, R.H. Brown, K.H. Baines, B.J. Buratti, R.N. Clark, M. Crapeau, P.J. Encrenaz, R. Jaumann, D. Geudtner, F. Paganelli, L. Soderblom, G. Tobie, S. Wall, Mapping and interpretation of Sinlap crater on Titan using Cassini VIMS and RADAR data. J. Geophys. Res. **113**, E04003 (2008). https://doi.org/10.1029/2007JE002965

E. Lellouch, Titan's zoo of clouds. Science **311**, 186–187 (2006)

M.T. Lemmon, E. Karkoschka, M. Tomasko, Titan's rotation—surface feature observed. Icarus **103**(2), 329–332 (1993)

J.S. Lewis, Satellites of the outer planets: their physical and chemical nature. Icarus **15**, 174–185 (1971)

Z.Y-C. Liu, J. Radebaugh, R.A. Harris, E.H. Christiansen, C.D. Neish, R.L. Kirk, R.D. Lorenz (the Cassini RADAR Team), The tectonics of Titan: global structural mapping from Cassini RADAR. Icarus **270**, 14–29 (2016a)

Z.Y.-C. Liu, J. Radebaugh, R.A. Harris, E.H. Christiansen, S. Rupper, Role of fluids in the tectonic evolution of Titan. Icarus **270**, 2–13 (2016b)

R.M.C. Lopes, K.L. Mitchell, E.R. Stofan, J.I. Lunine, R. Lorenz, F. Paganelli, R.L. Kirk, C.A. Wood, S.D. Wall, L.E. Robshaw, A.D. Fortes, C.D. Neish, J. Radebaugh, E. Reffet, S.J. Ostro, C. Elachi, M.D. Allison, Y. Anderson, R. Boehmer, G. Boubin, P. Callahan, P. Encrenaz, E. Flamini, G. Francescetti, Y. Gim, G. Hamilton, S. Hensley, M.A. Janssen, W.T.K. Johnson, K. Kelleher, D.O. Muhleman, G. Ori, R. Orosei, G. Picardi, F. Posa, L.E. Roth, R. Seu, S. Shaffer, L.A. Soderblom, B. Stiles, S. Vetrella, R.D. West, L. Wye, H.A. Zebker, Cryovolcanic features on Titan's surface as revealed by the Cassini Titan Radar Mapper. Icarus **186**, 395–412 (2007)

R.M.C. Lopes, E.R. Stofan, R. Peckyno, J. Radebaugh, K.L. Mitchell, G. Mitri, C.A. Wood, R.L. Kirk, S.D. Wall, J.I. Lunine, A. Hayes, R. Lorenz, T. Farr, L. Wye, J. Craig, R.J. Ollerenshaw, M. Janssen, A. LeGall, F. Paganelli, R. West, B. Stiles, P. Callahan, Y. Anderson, P. Valora, L. Soderblom (the Cassini RADAR Team), Distribution and interplay of geologic processes on Titan from Cassini RADAR data. Icarus **205**, 540–588 (2010). https://doi.org/10.1016/j.icarus.2009.08.010

R.M.C. Lopes, S.A. Fagents, K.L. Mitchell, T.K.P. Gregg, Planetary volcanism, in *Modeling Volcanic Processes*, ed. by S.A. Fagents, T.K.P. Gregg, R.M.C. Lopes (Cambridge University Press, Cambridge, 2013a), pp. 384–413

R.M.C. Lopes, R.L. Kirk, K.L. Mitchell, A. LeGall, J.W. Barnes, A. Hayes, J. Kargel, L. Wye, J. Radebaugh, E.R. Stofan, M. Janssen, C. Neish, S. Wall, C.A. Wood, J.I. Lunine, M. Malaska, Cryovolcanism on Titan: new results from Cassini RADAR and VIMS. J. Geophys. Res., Planets **118**, 1–20 (2013b). https://doi.org/10.1002/jgre.20062

R.M.C. Lopes, M.J. Malaska, A. Solomonidou, A. LeGall, M.A. Janssen, C. Neish, E.P. Turtle, S.P.D. Birch, A.G. Hayes, J. Radebaugh, A. Coustenis, A. Schoenfeld, B.W. Stiles, R.L. Kirk, K.L. Mitchell, E.R. Stofan, K.J. Lawrence (the Cassini RADAR Team), Nature, distribution, and origin of Titan's undifferentiated plains ("blandlands"). Icarus **270**, 162–182 (2016)

J.M. Lora, J.I. Mitchell, Titan's asymmetric lake distribution mediated by methane transport due to atmospheric eddies. Geophys. Res. Lett. **42**(15), 6213–6220 (2015)

J.M. Lora, J.I. Lunine, J.L. Russell, A.G. Hayes, Simulations of Titan's paleoclimate. Icarus **243**, 264–273 (2014)

R.D. Lorenz, The surface of Titan in the context of ESA's Huygens probe. ESA J. **17**, 275–292 (1993)

R.D. Lorenz, Pillow lava on Titan: expectations and constraints on cryovolcanic processes. Planet. Space Sci. **44**(9), 1021–1028 (1996)

R.D. Lorenz, Physics of saltation and sand transport on Titan: a brief review. Icarus **230**, 162–167 (2014)

R.D. Lorenz, A.G. Hayes, The growth of wind-waves in Titan's hydrocarbon seas. Icarus **219**(1), 468–475 (2012). https://doi.org/10.1016/j.icarus.2012.03.002

R.D. Lorenz, J.I. Lunine, Erosion on Titan: past and present. Icarus **196**, 79–91 (1996)

R.D. Lorenz, J.I. Lunine, Titan's surface before Cassini. Planet. Space Sci. **53**, 557–576 (2005)

R.D. Lorenz, J. Radebaugh, Global pattern of Titan's dunes: radar survey from the Cassini prime mission. Geophys. Res. Lett. **36**(3), L03202 (2009)

R.D. Lorenz, J.R. Zimbelman, *Dune Worlds: How Windblown Sand Shapes Planetary Landscapes* (Springer, Berlin, 2014)

R.D. Lorenz, J.I. Lunine, J.A. Grier, M.A. Fisher, Prediction of aeolian features on planets: application to Titan paleoclimatology. J. Geophys. Res., Planets **100**(E12), 26377–26386 (1995)

R.D. Lorenz, C.P. McKay, J.I. Lunine, Photochemically driven collapse of Titan's atmosphere. Science **275**, 642–644 (1997)

R.D. Lorenz, G. Biolluz, P. Encrenaz, M.A. Janssen, R.D. West, D.O. Muhleman, Cassini RADAR: prospects for Titan surface investigations using the microwave radiometer. Planet. Space Sci. **51**(4–5), 353–364 (2003)

R.D. Lorenz, C.A. Griffith, J.I. Lunine, C.P. McKay, N.O. Rennò, Convective plumes and the scarcity of Titan's clouds. Geophys. Res. Lett. **32**(1), L01201 (2005)

R.D. Lorenz, S. Wall, J. Radebaugh, G. Boubin, E. Reffet, M. Janssen, E. Stofan, R. Lopes, R. Kirk, C. Elachi, J. Lunine, The sand seas of Titan: Cassini RADAR observations of longitudinal dunes. Science **312**(5774), 724–727 (2006)

R.D. Lorenz, C.A. Wood, J.I. Lunine, S.D. Wall, R.M. Lopes, K.L. Mitchell, F. Paganelli, Y.Z. Anderson, L. Wye, C. Tsai, H. Zebker, E.R. Stofan, Titan's young surface: initial impact crater survey by Cassini RADAR and model comparison. Geophys. Res. Lett. **34**, L07204 (2007)

R.D. Lorenz, B. Stiles, R.L. Kirk, M. Allison, P. Persi del Marmo, L. Iess, J.I. Lunine, S.J. Ostro, S. Hensley, Titan's rotation reveals an internal ocean and changing zonal winds. Science **319**, 1649–1651 (2008a)

R.D. Lorenz, K.L. Mitchell, R.L. Kirk, A.G. Hayes, H.A. Zebker, P. Paillou, J. Radebaugh, J.I. Lunine, M.A. Janssen, S.D. Wall, R.M. Lopes, B. Stiles, S. Ostro, G. Mitri, E.R. Stofan (the Cassini RADAR Team), Titan's inventory of organic surface materials. Geophys. Res. Lett. **35**, L02206 (2008b). https://doi.org/10.1029/2007GL032118

R.D. Lorenz, R.M. Lopes, F. Paganelli, J.I. Lunine, R.L. Kirk, K.L. Mitchell, L.A. Soderblom, E.R. Stofan, G. Ori, M. Myers, H. Miyamoto, J. Radebaugh, B. Stiles, S.D. Wall, C.A. Wood (the Cassini RADAR Team), Fluvial channels on Titan: initial Cassini RADAR observations. Planet. Space Sci. **56**, 1132–1144 (2008c)

R.D. Lorenz, P. Claudin, B. Andreotti, J. Radebaugh, T. Tokano, A 3 km atmospheric boundary layer on Titan indicated by dune spacing and Huygens data. Icarus **205**, 719–721 (2010). https://doi.org/10.1016/j.icarus.2009.08.002

R.D. Lorenz et al., A global topographic map of Titan. Icarus **255**, 367–377 (2013). https://doi.org/10.1016/j.icarus.2013.04.002

A. Lucas, S. Rodriguez, C. Narteau, B. Charnay, S.C. Pont, T. Tokano, A. Garcia, M. Thiriet, A.G. Hayes, R.D. Lorenz, O. Aharonson, Growth mechanisms and dune orientation on Titan. Geophys. Res. Lett. **41**(17), 6093–6100 (2014). https://doi.org/10.1002/2014GL060971

J.I. Lunine, R.D. Lorenz, Rivers, lakes, dunes, and rain: crustal processes in Titan's methane cycle. Annu. Rev. Earth Planet. Sci. **37**(1), 299–320 (2009)

J.I. Lunine, R.D. Lorenz, W.K. Hartmann, Some speculations on Titans past, present and future. Planet. Space Sci. **46**(9–10), 1099–1107 (1998)

J.I. Lunine, C. Elachi, S.D. Wall, M.A. Janssen, M.D. Allison, Y. Anderson et al., Titan's diverse landscapes as evidenced by Cassini RADAR's third and fourth looks. Icarus **195**, 415–433 (2008)

S.M. MacKenzie, J.W. Barnes, C. Sotin, J.M. Soderblom, S. Le Mouélic, S. Rodriguez, K.H. Baines, B.J. Buratti, R.N. Clark, P.D. Nicholson, T.B. McCord, Evidence of Titan's climate history from evaporite distribution. Icarus **243**, 191–207 (2014)

M.J. Malaska, R. Hodyss, Dissolution of benzene, naphthalene, and biphenyl in a simulated Titan lake. Icarus **242**, 74–81 (2014). https://doi.org/10.1016/j.icarus.2014.07.022

M. Malaska, J. Radebaugh, R. Lorenz, K. Mitchell, T. Farr, E. Stofan, Identification of karst-like terrain on Titan from valley analysis, in *Lunar and Planetary Science Conference*, vol. 41 (2010). Abstract 1544

M. Malaska, J. Radebaugh, K. Mitchell, R. Lopes, S. Wall, R. Lorenz, Surface dissolution model for Titan karst, in *First International Planetary Cave Research Workshop*, October 2011 (2011a). Abstract 8018

M. Malaska, J. Radebaugh, A. Le Gall, K. Mitchell, R. Lopes, S. Wall, High-volume meandering channels in Titan's south polar region, in *Lunar and Planetary Science Conference* (2011b). Abstract 1562

M.J. Malaska, R.M. Lopes, A.G. Hayes, J. Radebaugh, R.D. Lorenz, E.P. Turtle, Material transport map of Titan: the fate of dunes. Icarus **270**, 183–196 (2016a). https://doi.org/10.1016/j.icarus.2015.09.029

M.J. Malaska, R.M.C. Lopes, D.A. Williams, C.D. Neish, A. Solomonidou, J.M. Soderblom, A.M. Schoenfeld, S.P.D. Birch, A.G. Hayes, A. Le Gall, M.A. Janssen, T.G. Farr, R.D. Lorenz, J. Radebaugh, E.P. Turtle, Geomorphological map of the Afekan Crater region, Titan: terrain relationships in the equatorial and mid-latitude regions. Icarus **270**, 130–161 (2016b). https://doi.org/10.1016/j.icarus.2016.02.021

M.J. Malaska, R. Hodyss, J.I. Lunine, A.G. Hayes, J.D. Hofgartner, G. Hollyday, R.D. Lorenz, Laboratory measurements of nitrogen dissolution in Titan lake fluids. Icarus **289**, 94–105 (2017a). https://doi.org/10.1016/j.icarus.2017.01.033

M.J. Malaska, R.M.C. Lopes, K.L. Mitchell, J. Radebaugh, T. Verlander, A. Schoenfeld, Classification of labyrinth terrains on Titan, in *Lunar and Planetary Science Conference* (2017b). Abstract 2406

M. Mastrogiuseppe, V. Poggiali, A. Hayes, R. Lorenz, J. Lunine, G. Picardi, R. Seu, E. Flamini, G. Mitri, C. Notarnicola, Ph. Paillou, H. Zebker, The bathymetry of a Titan sea. Geophys. Res. Lett. **41**(5), 1432–1437 (2014)

M. Mastrogiuseppe, A. Hayes, V. Poggiali, R. Seu, J.I. Lunine, J.D. Hofgartner, Radar sounding using the Cassini altimeter: waveform modeling and Monte Carlo approach for data inversion of observations of Titan's seas. IEEE Trans. Geosci. Remote Sens. **54**(10), 5646–5656 (2016)

M. Mastrogiuseppe, A.G. Hayes, V. Poggiali, J.I. Lunine, R.D. Lorenz, R. Seu, A. Le Gall, C. Notarnicola, K.L. Mitchell, M. Malaska, S.P.D. Birch, Bathymetry and composition of Titan's Ontario Lacus derived from Monte Carlo-based waveform inversion of Cassini RADAR altimetry data. Icarus **300**, 203–209 (2018)

T.B. McCord, G.B. Hansen, B.J. Buratti, R.N. Clark, D.P. Cruikshank, E. D'Aversa, C.A. Griffith, E.K.H. Baines, R.H. Brow, C.M. Dalle Ore, G. Filacchione, V. Formisano, C.A. Hibbitts, R. Jaumann, J.I. Lunine, R.M. Nelson, C. Sotin (the Cassini VIMS Team), Composition of Titan's surface from Cassini VIMS. Planet. Space Sci. **54**, 1524–1539 (2006). https://doi.org/10.1016/j.pss.2006.06.007

T.B. McCord, P. Hayne, J.-P. Combe, G.B. Hansen, J. Barnes, S. Rodriguez, S. Le Mouelic, K. Baines, B. Buratti, C. Sotin, P. Nicholson, R. Jaumann, R. Nelson (Cassini VIMS Team), Titan's surface: search for spectral diversity and composition using the Cassini VIMS investigation. Icarus **194**, 212–242 (2008)

G.D. McDonald, A.G. Hayes, R.C. Ewing, J.M. Lora, C.E. Newman, T. Tokano, A. Lucas, A. Soto, G. Chen, Variations in Titan's dune orientations as a result of orbital forcing. Icarus **270**, 197–210 (2016)

J. Méndez-Harper, G.D. McDonald, J. Dufek, M.J. Malaska, D.M. Burr, A.G. Hayes, J. McAdams, J.J. Wray, The electrified sands of Titan. Nat. Geosci. **10**, 260–265 (2017). https://doi.org/10.1038/ngeo2921

R. Meriggiola, L. Iess, B.W. Stiles, J.I. Lunine, G. Mitri, The rotational dynamics of Titan from Cassini RADAR images. Icarus **275**, 183–192 (2016)

J.L. Mitchell, The drying of Titan's dunes: Titan's methane hydrology and its impact on atmospheric circulation. J. Geophys. Res., Planets **113**(E8), E08015 (2008)

J.L. Mitchell, J.M. Lora, The climate of Titan. Ann. Rev. Earth Planet. Sci. **44**, 353–380 (2016). https://doi.org/10.1146/annurev-earth-060115-012428

K.L. Mitchell, M.B. Barmatz, C.S. Jamieson, R.D. Lorenz, J.I. Lunine, Laboratory measurements of cryogenic liquid alkane microwave absorptivity and implications for the composition of Ligeia Mare, Titan. Geophys. Res. Lett. **42**, 1340–1345 (2015)

G. Mitri, M.T. Bland, A.P. Showman, J. Radebaugh, B. Stiles, R.M.C. Lopes, J.I. Lunine, R.T. Pappalardo, Mountains on Titan: modeling and observations. J. Geophys. Res. **115**, E10002 (2010). https://doi.org/10.1029/2010JE003592

G. Mitri et al., Shape, topography, gravity anomalies and tidal deformation of Titan. Icarus **236**, 169–177 (2014)

J.M. Moore, R.T. Pappalardo, Titan: an exogenic world? Icarus **212**, 790–806 (2011)

J.M. Moore, A.D. Howard, A.M. Morgan, The landscape of Titan as witness to its climate evolution. J. Geophys. Res., Planets **119**, 2060–2077 (2014). https://doi.org/10.1002/2014JE004608

C.D. Neish, R.D. Lorenz, Titan's global crater population: a new assessment. Planet. Space Sci. **60**(1), 26–33 (2012)

C.D. Neish, R.D. Lorenz, Elevation distribution of Titan's craters suggests extensive wetlands. Icarus **228**, 27–34 (2014)

C.D. Neish, R.D. Lorenz, R.L. Kirk, L.C. Wye, Radarclinometry of the sand seas of Africa's Namibia and Saturn's moon Titan. Icarus **208**, 385–394 (2010)

C.D. Neish, R.L. Kirk, R.D. Lorenz, V.J. Bray, P. Schenk, B.W. Stiles et al., Crater topography on Titan: implications for landscape evolution. Icarus **223**, 82–90 (2013)

C.D. Neish, J.W. Barnes, C. Sotin, S. MacKenzie, J.M. Soderblom, S. Le Mouélic et al., Spectral properties of Titan's impact craters imply chemical weathering of its surface. Geophys. Res. Lett. **42**, 3746–3754 (2015)

C.D. Neish, J.L. Molaro, J.M. Lora, A.D. Howard, R.L. Kirk, P. Schenk et al., Fluvial erosion as a mechanism for crater modification on Titan. Icarus **270**, 114–129 (2016)

R.M. Nelson, L.W. Kamp, D.L. Matson, P.G.J. Irwin, K.H. Baines, M.D. Boryta, F.E. Leader, R. Jaumann, W.D. Smythe, C. Sotin, R.N. Clark, D.P. Cruikshank, P. Drossart, J.C. Pearl, B.W. Hapke, J. Lunine, M. Combes, G. Bellucci, J.-P. Bibring, F. Capaccioni, P. Cerroni, A. Coradini, V. Formisano, G. Filacchione, R.Y. Langevin, T.B. McCordo, V. Mennella, P.D. Nicholson, B. Sicardy, Saturn's Titan: surface change, ammonia, and implications for atmospheric and tectonic activity. Icarus **199**, 429–441 (2009a). https://doi.org/10.1016/j.icarus.2008.08.013

R.M. Nelson, L.W. Kamp, R.M.C. Lopes, D.L. Matson, R.L. Kirk, B.W. Hapke, S.D. Wall, M.D. Boryta, F.E. Leader, W.D. Smythe, K.L. Mitchell, K.H. Baines, R. Jaumann, C. Sotin, R.N. Clark, D.P. Cruikshank, P. Drossart, J.I. Lunine, M. Combes, G. Bellucci, J-P. Bibring, F. Capaccioni, P. Cerroni, A. Coradini, V. Formisano, G. Filacchione, Y. Langevin, T.B. McCord, V. Mennella, P.D. Nicholson, B. Sicardy, P.G.J. Irwin, Photometric changes on Saturn's moon Titan: evidence for cryovolcanism. Geophys. Res. Lett. **36**, L04202 (2009b). https://doi.org/10.1029/2008GL036206

H.B. Niemann, S.K. Atreya, S.J. Bauer, G.R. Carignan, J.E. Demick, R.L. Frost, D. Gautier, J.A. Haberman, D.N. Harpold, D.M. Hunten, G. Israel, J.I. Lunine, W.T. Kasprzak, T.C. Owen, M. Paulkovich, F. Raulin, E. Raaen, S.H. Way, Huygens Probe Gas Chromatograph Mass Spectrometer: the atmosphere and surface of Titan. Nature (2005). https://doi.org/10.1038/nature04122

F. Nimmo, B.G. Bills, Shell thickness variations and the long-wavelength topography of Titan. Icarus **208**, 896–904 (2010)

C. Nixon, R. Clark, R. Courtin, A. Hayes, R. Lopes, R. Yelle, C. Sotin, A. Rymer, R. Johnson, R. Lorenz, M. Mastrogiuseppe, H. Smith, D. Strobel, R. Achterberg, A. Buch, K. Mandt, D. Mitchell, F. Raulin, E. Turtle, L. Iess, V. Vuitton, A. Solomonidou, R. West, P. Coll, Titan's cold case files—outstanding questions after Cassini-Huygens. Planet. Space Sci. **155**, 50–72 (2018)

D. Northrup, J. Radebaugh, E.H. Christiansen, S. Tass, L. Kerber, Yardang and dune classification on Titan through length, width, and Sinuosity, in *49th Lunar and Planetary Science Conference*, 19–23 March, 2018, The Woodlands, Texas. LPI Contribution, vol. 2083 (2018)

F. Paganelli, M.A. Janssen, B. Stiles, R. West, R.D. Lorenz, J.I. Lunine, S.D. Wall, P. Callahan, R.M. Lopes, E. Stofan, R.L. Kirk, W.T.K. Johnson, L. Roth, C. Elachi (the Cassini Radar Team), Titan's surface from the Cassini Radar SAR and high resolution radiometry data of the first five flybys. Icarus **191**, 211–222 (2007)

F. Paganelli, M.A. Janssen, R.M. Lopes, E. Stofan, S.D. Wall, R.D. Lorenz, J.I. Lunine, R.L. Kirk, L. Roth, C. Elachi (the Cassini Radar Team), Titan's surface from the Cassini RADAR radiometry data during SAR mode. Planet. Space Sci. **56**, 100–108 (2008)

P. Paillou, M. Crapeau, C. Elachi, S. Wall, P. Encrenaz, Models of SAR backscattering for bright flows and dark spots on Titan. J. Geophys. Res. **111**, E11011 (2006). https://doi.org/10.1029/2006JE002724

P. Paillou, J.I. Lunine, G. Ruffié, P. Encrenaz, S.D. Wall, R.D. Lorenz, M.A. Janssen, Microwave dielectric constant of Titan-relevant materials. Geophys. Res. Lett. **35**, L18202 (2008)

P. Paillou, D. Bernard, J. Radebaugh, R. Lorenz, A. Le Gall, T. Farr, Modeling the SAR backscatter of linear dunes on Earth and Titan. Icarus **230**, 208–214 (2014)

P. Paillou, B. Seignovert, J. Radebaugh, S. Wall, Radar scattering of linear dunes and mega-yardangs: application to Titan. Icarus **270**, 211–221 (2016)

J.T. Perron, M.P. Lamb, C.D. Koven, I.Y. Fung, E. Yager, M. Adamkovics, Valley formation and methane precipitation rates on Titan. J. Geophys. Res. **111**, E11001 (2006)

V. Poggiali, M. Mastrogiuseppe, A.G. Hayes, R. Seu, S.P.D. Birch, R. Lorenz, C. Grima, J.D. Hofgartner, Liquid-filled canyons on Titan. Geophys. Res. Lett. **43**, 7887–7894 (2016)

C.C. Porco, R.A. West, S. Squyres, A. McEwen, T. Peter, C.D. Murray, A. Delgenio, A.P. Ingersoll, T.V. Johnson, G. Neukum et al., Cassini imaging science: instrument characteristics and anticipated scientific investigations at Saturn. Space Sci. Rev. **115**(1–4), 363–497 (2004). https://doi.org/10.1007/s11214-004-1456-7

C.C. Porco, E. Baker, J. Barbara, K. Beurle, A. Brahic, J.A. Burns, S. Charnoz, N. Cooper, D.D. Dawson, A.D. Del Genio, T. Denk, L. Dones, U. Dyudina, M.W. Evans, S. Fussner, B. Giese, K. Grazier, P. Helfenstein, A.P. Ingersoll, R.A. Jacobson, T.V. Johnson, A. McEwen, C.D. Murray, G. Neukum, W.M. Owen, J. Perry, T. Roatsch, J. Spitale, S. Squyres, P. Thomas, M. Tiscareno, E.P. Turtle, A.R. Vasavada, J. Veverka, R. Wagner, R. West, Imaging of Titan from the Cassini spacecraft. Nature **434**, 159–168 (2005). https://doi.org/10.1038/nature03436

J. Radebaugh, Dunes on Saturn's moon Titan at the end of the Cassini Equinox Mission. Aeolian Res. **11**, 23–41 (2013)

J. Radebaugh, R.D. Lorenz, R.L. Kirk, J.I. Lunine, E.R. Stofan, R.M.C. Lopes, S.D. Wall (the Cassini Radar Team), Mountains on Titan observed by Cassini Radar. Icarus **192**, 77–91 (2007). https://doi.org/10.1016/j.icarus.2007.06.020

J. Radebaugh, R. Lorenz, J. Lunine, S. Wall, G. Boubin, E. Reffet, R. Kirk, R. Lopes, E. Stofan, L. Soderblom, M. Allison, M. Janssen, P. Paillou, P. Callahan (the Cassini Radar Team), Dunes on Titan observed by Cassini Radar. Icarus **194**, 690–703 (2008). https://doi.org/10.1016/j.icarus.2007.10.015

J. Radebaugh, R. Lorenz, T. Farr, P. Paillou, C. Savage, C. Spencer, Linear dunes on Titan and Earth: initial remote sensing comparisons. Geomorphology **121**, 122–132 (2010). https://doi.org/10.1016/j.geomorph.2009.02.022

J. Radebaugh, R.D. Lorenz, S.D. Wall, R.L. Kirk, C.A. Wood, J.I. Lunine, E.R. Stofan, R.M.C. Lopes, P. Valora, T.G. Farr, A.G. Hayes, B. Stiles, G. Mitri, H. Zebker, M. Janssen, L. Wye, A. Le Gall, K.L. Mitchell, F. Paganelli, R.D. West, E.L. Schaller (the Cassini RADAR Team), Regional geomorphology and history of Titan's Xanadu province. Icarus **211**, 672–685 (2011)

J. Radebaugh, D. Ventra, R.D. Lorenz, T. Farr, R. Kirk, A. Hayes, M.J. Malaska, S. Birch, Z.Y-C. Liu, J. Lunine, J. Barnes, A. Le Gall, R. Lopes, E. Stofan, S. Wall, P. Paillou, Alluvial and fluvial fans on Saturn's moon Titan reveal processes, materials and regional geology, in *Geology and Geomorphology of Alluvial and Fluvial Fans: Terrestrial and Planetary Perspectives*, ed. by D. Ventra, L.E. Clarke. Special Publications, vol. 440 (Geological Society, London, 2016). https://doi.org/10.1144/SP440.6

P. Rannou, F. Montmessin, F. Hourdin, S. Lebonnois, The latitudinal distribution of clouds on Titan. Science **311**(5758), 201–205 (2006)

F. Raulin, Organic chemistry in the oceans of Titan. Adv. Space Res. **7**(5), (5)71–(5)81 (1987)

L.A. Richardson, J.W. Hartwig, J.W. Leachman, Experimental PρT-x measurements of liquid methane-ethane-nitrogen mixtures. Fluid Phase Equilib. **462**, 38–43 (2018). https://doi.org/10.1016/j.fluid.2018.01.023

S. Rodriguez, A. Garcia, A. Lucas, T. Appéré, A. Le Gall, E. Reffet, L. Le Corre, S. Le Mouélic, T. Cornet, S. Courrech du Pont, C. Narteau, O. Bourgeois, J. Radebaugh, K. Arnold, J.W. Barnes, K. Stephan, R. Jaumann, C. Sotin, R.H. Brown, R.D. Lorenz, E.P. Turtle, Global mapping and characterization of Titan's dune fields with Cassini: correlation between RADAR and VIMS observations. Icarus **230**, 168–179 (2014)

D.M. Rubin, P.A. Hesp, Multiple origins of linear dunes on Earth and Titan. Nat. Geosci. **2**(9), 653 (2009)

C. Sagan, S.F. Dermott, The tide in the seas of Titan. Nature **300**, 731–733 (1982)
C.J. Savage, J. Radebaugh, E.H. Christiansen, R.D. Lorenz, Implications of dune pattern analysis for Titan's surface history. Icarus **230**, 180–190 (2014)
E.L. Schaller, M.E. Brown, H.G. Roe, A.H. Bouchez, A large cloud outburst at Titan's south pole. Icarus **182**(1), 224–229 (2006)
L.R. Schurmeier, A.J. Dombard, Crater relaxation on Titan aided by low thermal conductivity sand infill. Icarus **305**, 314–323 (2018). https://doi.org/10.1016/j.icarus.2017.10.034
L. Schurmeier, A.J. Dombard, M. Malaska, J. Radebaugh, Are Titan's radial labyrinth terrains surface expressions of large laccoliths? in *American Geophysical Union Fall Meeting*, New Orleans (2017)
L. Schurmeier, A.J. Dombard, J. Radebaugh, M. Malaska, Intrusive and extrusive cryovolcanism and the composition of Titan's icy crust, in *Lunar and Planetary Science Conference*, vol. 49 (2018). Abstract 2934
W.D. Sears, Tidal dissipation in oceans on Titan. Icarus **113**, 39–56 (1995)
P.H. Smith, M.T. Lemmon, R.D. Lorenz, L.A. Sromovsky, J.J. Caldwell, M.D. Allison, Titan's surface, revealed by HST imaging. Icarus **119**(2), 336–349 (1996)
L. Soderblom, J. Anderson, K. Baines, J. Barnes, J. Barrett, R. Brown, B. Buratti, R. Clark, D. Cruikshank, C. Elachi, M. Janssen, R. Jaumann, R. Kirk, E. Karkoschka, S. Lemouelic, R. Lopes, R. Lorenz, J. Lunine, T. McCord, P. Nicholson, J. Radebaugh, B. Rizk, C. Sotin, E. Stofan, T. Sucharski, M. Tomasko, S. Wall, Correlations between Cassini VIMS spectra and RADAR SAR images: implications for Titan's surface composition and the character of the Huygens Probe landing site. Planet. Space Sci. **55**, 2025–2036 (2007)
L.A. Soderblom, R.H. Brown, J.M. Soderblom, J.W. Barnes, R.L. Kirk, C. Sotin, R. Jaumann, D.J. MacKinnon, D.W. Mackowski, K.H. Baines, B.J. Buratti, R.N. Clark, P.D. Nicholson, The geology of Hotei Regio, Titan: correlation of Cassini VIMS and RADAR. Icarus **204**, 610–618 (2009). https://doi.org/10.1016/j.icarus.2009.07.033
J.M. Soderblom, R.H. Brown, L.A. Soderblom, J.W. Barnes, R. Jaumann, S. Le Mouélic et al., Geology of the Selk crater region on Titan from Cassini VIMS observations. Icarus **208**, 905–912 (2010)
J.M. Soderblom, J.W. Barnes, R.H. Brown, V. Chevrier, K. Farnsworth, L.A. Soderblom, Evidence for frozen hydrocarbons on Titan, in *American Astronomical Society, DPS Meeting*, vol. 48 (2016)
F. Sohl, H. Hussmann, B. Schwentker, T. Spohn, R.D. Lorenz, Interior structure models and tidal Love numbers of Titan. J. Geophys. Res. **108**(E12), 5130 (2003). https://doi.org/10.1029/2003JE002044
F. Sohl, A. Solomonidou, F.W. Wagner, A. Coustenis, H. Hussmann, D. Schulze-Makuch, Tidal stresses on Titan and implications for its geology and habitability. J. Geophys. Res. **119**, 1013–1036 (2014)
A. Solomonidou et al., Surface albedo spectral properties of geologically interesting areas on Titan. J. Geophys. Res. **119**, 1729–1747 (2014)
A. Solomonidou, A. Coustenis, M. Hirtzig, S. Rodriguez, K. Stephan, R.M.C. Lopes, P. Drossart, C. Sotin, S. Le Mouélic, K. Lawrence, E. Bratsolis, R. Jaumann, R.H. Brown, Temporal variations of Titan's surface with Cassini/VIMS. Icarus **270**, 85–99 (2016)
A. Solomonidou, A. Coustenis, R.M.C. Lopes, M. Malaska, S. Rodriguez, P. Drossart, C. Elachi, B. Schmitt, S. Philippe, M. Janssen, M. Hirtzig, S. Wall, C. Sotin, K. Lawrence, N. Altobelli, E. Bratsolis, J. Radebaugh, K. Stephan, R.H. Brown, S. Le Mouélic, A. Le Gall, E.V. Villanueva, J.F. Brossier, A.A. Bloom, O. Witasse, C. Matsoukas, A. Schoenfeld, The spectral nature of Titan's major geomorphological units: constraints on surface composition. J. Geophys. Res., Planets (2018). https://doi.org/10.1002/2017JE005477
C. Sotin, R. Jaunmann, B.J. Buratti, R.H. Brown, R.N. Clark, L.A. Soderblom, K.H. Baines, G. Bellucci, J-P. Bribing, F. Capaccioni, P. Cerroni, A. Coradini, D.P. Cruikshank, P. Drossart, V. Formisano, Y. Langevin, D.L. Matson, T.B. McCord, R.M. Nelson, P.D. Nicholson, B. Sicardy, S. LeMouelic, S. Rodriguez, K. Stephan, C.K. Scholz, Release of volatiles from a possible cryovolcano from near-infrared imaging of Titan. Nature **435**, 786–789 (2005)
K. Stephan et al., Specular reflection on Titan: liquids in Kraken Mare. Geophys. Res. Lett. **37**, L07104 (2010). https://doi.org/10.1029/2009GL042312
B.W. Stiles, R.L. Kirk, R.D. Lorenz, S. Hensley, E. Lee, S.J. Ostro, M.D. Allison, P.S. Callahan, Y. Gim, L. Iess, Determining Titan's spin state from Cassini radar images. Astron. J. **135**(5), 1669–1680 (2008)
B.W. Stiles, S. Hensley, Y. Gim, D.M. Bates, R.L. Kirk, A. Hayes, J. Radebaugh, R.D. Lorenz, K.L. Mitchell, P.S. Callahan, H. Zebker, W.T.K. Johnson, S.D. Wall, J.I. Lunine, C.A. Wood, M. Janssen, F. Pelletier, R.D. West, C. Veeramacheneni, Determining Titan surface topography from Cassini SAR data. Icarus **102**, 584–598 (2009). https://doi.org/10.1016/j.icarus.2009.03.032
B. Stiles, R. Kirk, R. Lorenz, S. Hensley, E. Lee, S. Ostro, M. Allison, P. Callahan, Y. Gim, L. Iess, P. Perci del Marmo, G. Hamilton, W. Johnson, R. West (Cassini RADAR Team), Determining Titan's spin state from Cassini Radar images. Astron. J. **139**(1), 311 (2010)

E.R. Stofan, J.I. Lunine, R. Lopes, F. Paganelli, R.D. Lorenz, C.A. Wood, R. Kirk, S. Wall, C. Elachi, L.A. Soderblom, S. Ostro, M. Janssen, J. Radebaugh, L. Wye, H. Zebker, Y. Anderson, M. Allison, R. Boehmer, P. Callahan, P. Encrenaz, E. Flamini, G. Francescetti, Y. Gim, G. Hamilton, S. Hensley, W.T.K. Johnson, K. Kelleher, D. Muhleman, G. Picardi, F. Posa, L. Roth, R. Seu, S. Shaffer, B. Stiles, S. Vetrella, R. West, Mapping of Titan: results from the first Titan Radar passes. Icarus **185**, 443–456 (2006)

E.R. Stofan, C. Elachi, J.I. Lunine, R.D. Lorenz, B. Stiles, K.L. Mitchell, S. Ostro, L. Soderblom, C. Wood, H. Zebker, S. Wall, M. Janssen, R. Kirk, R. Lopes, F. Paganelli, J. Radebaugh, L. Wye, Y. Anderson, M. Allison, R. Boehmer, P. Callahan, P. Encrenaz, E. Flamini, G. Francescetti, Y. Gim, G. Hamilton, S. Hensley, W.T.K. Johnson, K. Kelleher, D. Muhleman, P. Paillou, G. Picardi, F. Posa, L. Roth, R. Seu, S. Shaffer, S. Vetrella, R. West, The lakes of Titan. Nature **445**, 61–64 (2007). https://doi.org/10.1038/nature05438

G. Tobie, J.I. Lunine, C. Sotin, Episodic outgassing as the origin of atmospheric methane on Titan. Nature **440**, 61–64 (2006)

G. Tobie, J.I. Lunine, J. Monteux, O. Mousis, F. Nimmo, The origin and evolution of Titan, in *Titan: Interior, Surface, Atmosphere, and Space Environment*, ed. by I. Müller-Wodarg, C.A. Griffith, E. Lellouch, T.E. Cravens (Cambridge University Press, Cambridge, 2014). https://doi.org/10.1017/CBO9780511667398

T. Tokano, Meteorological assessment of the surface temperatures on Titan: constraints on the surface type. Icarus **173**, 222–242 (2005)

T. Tokano, Dune-forming winds on Titan and the influence of topography. Icarus **194**(1), 243–262 (2008)

T. Tokano, Relevance of fast westerlies at equinox for the eastward elongation of Titan's dunes. Aeolian Res. **2**(2–3), 113–127 (2010)

M. Tomasko, B. Archinal, T. Becker, B. Bézard, M. Bushroe, M. Combes, D. Cook, A. Coustenis, C. de Bergh, L. Dafoe, L. Doose, S. Douté, A. Eibl, S. Engel, F. Gliem, B. Grieger, K. Holso, E. Howington-Kraus, E. Karkoschka, H. Keller, R. Kirk, R. Kramm, M. Küppers, P. Lanagan, E. Lellouch, M. Lemmon, J. Lunine, E. McFarlane, J. Moores, M. Prout, B. Rizk, M. Rosiek, P. Rueffer, S. Schröder, B. Schmitt, C. See, P. Smith, L. Soderblom, N. Thomas, R. West, Rain, winds, and haze during the Huygens probe descent to Titan's surface. Nature **438**, 765–778 (2005)

F. Tosi, R. Orosei, R. Seu, A. Coradini, J.I. Lunine, G. Filacchione, A.I. Gavrishin, F. Capaccioni, P. Cerroni, A. Adriani et al., Correlations between VIMS and RADAR data over the surface of Titan: implications for Titan's surface properties. Icarus **208**(1), 366–384 (2010)

H. Tsoar, Dynamic processes acting on a longitudinal (seif) dune. Sedimentology **30**, 567–578 (1983)

E.P. Turtle, J.E. Perry, A.S. McEwen, A.D. Del Genio, J. Barbara, R.A. West, D.D. Dawson, C.C. Porco, Cassini imaging of Titan's high-latitude lakes, clouds, and south-polar surface changes. Geophys. Res. Lett. **36**(2), L02204 (2009)

E.P. Turtle, J.E. Perry, A.G. Hayes, R.D. Lorenz, J.W. Barnes, A.S. McEwen, R.A. West, A.D. Del Genio, J.M. Barbara, E.L. Schaller, T.L. Ray, J.I. Lunine, R.M.C. Lopes, E.R. Stofan, Rapid and extensive surface changes near Titan's equator: evidence of April showers. Science **331**, 1414 (2011a). https://doi.org/10.1126/science.1201063. 2011

E.P. Turtle, J.E. Perry, A.G. Hayes, A.S. McEwen, Shoreline retreat at Titan's Ontario Lacus and Arrakis Planitia from Cassini Imaging Science Subsystem observations. Icarus **212**, 957–959 (2011b)

B. Ventura et al., Electromagnetic models and inversion techniques for Titan's Ontario Lacus depth estimation from Cassini RADAR data. Icarus **221**, 960–969 (2012). https://doi.org/10.1016/j.icarus.2012.09.011

G. Vixie, J.W. Barnes, B. Jackson, S. Rodriguez, S. Le Mouélic, C. Sotin, S. MacKenzie, P. Wilson, Possible temperate lakes on Titan. Icarus **257**, 313–323 (2015)

S.D. Wall, R.M. Lopes, E.R. Stofan, C.A. Wood, J.L. Radebaugh, B.W. Stiles, R.M. Nelson, L.W. Kamp, M.A. Janssen, R.L. Lorenz, J.I. Lunine, T.G. Farr, G. Mitri, P. Paillou, F. Paganelli, K.L. Mitchell, Cassini RADAR images at Hotei Arcus and Western Xanadu, Titan: evidence for recent cryovolcanic activity. Geophys. Res. Lett. **36**, L04203 (2009). https://doi.org/10.1029/2008GL036415

S. Wall, A. Hayes, C. Bristow, R. Lorenz, E. Stofan, J. Lunine, A. Le Gall, M. Janssen, R. Lopes, L. Wye, L. Soderblom, P. Paillou, O. Aharonson, H. Zebker, T. Farr, G. Mitri, R. Kirk, K. Mitchell, C. Notarnicola, D. Casarano, B. Ventura, Active shoreline of Ontario Lacus, Titan: a morphological study of the lake and its surroundings. Geophys. Res. Lett. **37**, L05202 (2010). https://doi.org/10.1029/2009GL041821

H.Y. Wei, C.T. Russell, M.K. Dougherty, F.M. Neubauer, Y.J. Ma, Upper limits on Titan's magnetic moment and implications for its interior. J. Geophys. Res. **115**, E10007 (2010)

C.A. Wood, Titan's great crustal thickening event and recent geologic history, in *LPSC*, vol. 49 (2018) p. 1343

C.A. Wood, K.L. Mitchell, R.M.C. Lopes, J. Radebaugh, E. Stoffan, J. Lunine (the Cassini RADAR Team), Volcanic Calderas in the North Polar Region of Titan, in *Lunar Planet. Sci. Conf. XXXVIII*, Houston, Texas (2007). Abstract 1454

C.A. Wood, R. Lorenz, R. Kirk, R. Lopes, K. Mitchell, E. Stofan, Impact craters on Titan. Icarus **206**, 334–344 (2010)

L.C. Wye, Radar Scatering from Titan and Saturn's Icy Satellites using the Cassini Spacecraft. Ph.D. thesis, Stanford University (2011)

L.C. Wye, H.A. Zebker, S.J. Ostro, R.D. West, Y. Gim, R.D. Lorenz (the Cassini Radar Team), Electrical properties of Titan's surface from Cassini RADAR scatterometer measurements. Icarus **188**, 367–385 (2007)

L.C. Wye, H.A. Zebker, R.D. Lorenz, Smoothness of Titan's Ontario Lacus: constraints from Cassini RADAR specular reflection data. Geophys. Res. Lett. **36**, 16201 (2009). https://doi.org/10.1029/2009GL039588

X. Yu, S.M. Hörst, C. He, N.T. Bridges, D.M. Burr, J.A. Sebree, J.K. Smith, The effect of adsorbed liquid and material density on saltation threshold: insight from laboratory and wind tunnel experiments. Icarus **297**, 97–109 (2017)

Y.L. Yung, M. Allen, J.P. Pinto, Photochemistry of the atmosphere of Titan: comparison between model and observations. Astrophys. J. Suppl. Ser. **55**, 465–506 (1984)

K. Zahnle, P. Schenk, H. Levison, L. Dones, Cratering rates in the outer Solar System. Icarus **163**, 263–289 (2003)

K. Zebker, Y-Q. Wong, Shape of Titan from Cassini radar elevation measurements and implications for interior structure and composition, in *AGU Fall Meeting*, Dec. 12–16, San Francisco (2016). Abstract P33F-01

H. Zebker, L. Wye, M. Janssen (Cassini Radar Team), Titan's surface from reconciled Cassini microwave reflectivity and emissivity observations. Icarus **194**(2), 704–710 (2008)

H.A. Zebker, B. Stiles, S. Hensley, R. Lorenz, R.L. Kirk, J.I. Lunine, Size and shape of Saturn's moon Titan. Science **324**, 921–923 (2009)

H. Zebker, A. Hayes, M. Janssen, A. Le Gall, R. Lorenz, L. Wye, Surface of Ligeia Mare, Titan, from Cassini altimeter and radiometer analysis. Geophys. Res. Lett. **41**, 308–313 (2014). https://doi.org/10.1002/2013GL058877